MAPPING AND MONITORING LAND TRANSFORMATION OF BOANE DISTRICT, MOZAMBIQUE (1980 – 2020), USING REMOTE SENSING

By:

Claudio Antonio Dengo (2416654)

Supervisor: Dr Elhadi Adam

Co-supervisor: Iqra Atif

A research report Submitted to the Faculty of Science, University of the Witwatersrand, Johannesburg, in fulfilment of the requirements for the degree of Masters of Science in Geographical Information Systems and Remote Sensing at the School of Geography, Archaeology & Environmental Studies

09 October 2023

DECLARATION

I declare this research report is my own, unaided work. It is submitted for the Degree of Master of Science in Geographical Information Systems and Remote Sensing to the University of the Witwatersrand, Johannesburg. It has not been submitted before for any degree or examination at any other University.

Cláudio António Dengo

____

(Signature of candidate)

09 October 2023

ABSTRACT

Although natural and environmental factors play a significant role in land transformation, human actions dominate. Therefore, to better understand the present land uses and predict the future, accurate information describing the nature and extent of changes over time is necessary and critical, especially for developing countries. It is estimated that these countries will account for 50% of the world's population growth in the next few years. Hence, this research was an attempt to assess and monitor land cover changes in Boane, Mozambique, over the past 40 years and predict what to expect in the next 30 years. This district has been challenged by a fast-growing population and land use dynamic, with quantitative information, driving forces and impacts remaining unknown. Through a supervised process in a cloud base Google Earth Engine platform, a set of five Landsat images at ten-year intervals were classified using a random forest algorithm. Seven land classes, i.e., agriculture, forest, built-up, barren, rock, wetland and water bodies, were extracted and compared through a pixel-by-pixel process as one of the most precise and accurate methods in remote sensing and geographic information system applications. The results indicate an active alternate between all land classes, with significant changes observed within agriculture, forest and build-up classes. As it is, while agriculture (-26.1%) and forest (-21.4%) showed a continuously decreasing pattern, build-up class (45.8%) increased tremendously. Consequently, over 69% of the forest area and 59% of the agricultural area shifted into build-up, i.e., was degraded or destroyed. Similarly, the conversion of barren land area (57.2%) and rock area (47.3%) into build-up indicates that those areas were cleaned. The overall classification accuracy averaged 90% and a kappa coefficient of 0.8779 were obtained. The CA-Markov model, used to assess future land uses, indicates that build-up will continue to increase significantly, covering 60% of the total area. From this finding, the land cover situation in the next 30 years will be critical if no action is taken to stop this uncontrolled urban sprawl. An adequate land use plan must be drawn, clearly indicating the locations for different activities and actions for implementation.

Keywords: Boane; Land use-land cover; Change detection; Land transformation, Google Earth Engine; Random forest.

ACKNOWLEDGEMENTS

I want to express my gratitude to my supervisors, Professor Elhadi Adams and Dr Iqra Atif, for their invaluable support and for sharing their knowledge and guidance. A thank goes to the University team for their time and support during lectures and along the way. To my fellow mates in RS and GIS Master, I appreciate your collaboration. To my family, I want to thank them for their unconditional support and encouragement. This research was fully supported by the National Statistical Institute of Mozambique. Landsat images were courtesy of the U.S. Geological Survey.

Claudio Dengo,

Johannesburg, 09 October 2023

Contents

LIST OF FIGURES

LIST OF ACRONYMS

ASTER	Advanced Spaceborne Thermal Emission and Reflection Radiometer
CA	Cellular Automata
ETM+	Enhanced Thematic Mapper Plus
GIS	Geographic Information System
GE	Google Earth
GEE	Google Earth Engine
LULC	Land Use Land Cover
MC	Markov Chain
OLI/TIRS	Operational Land Imager/Thermal Infrared Sensor
RS	Remote Sense
RF	Random Forest
Sq.km	Square Kilometre
TM	Thematic Mapper
USGS	United States Geological Survey

LIST OF TABLES

CHAPTER ONE

1. GENERAL INTRODUCTION

1.1. Background

Land is, among other resources, one of the most valuable on earth, as humans rely on its use for social and economic development, and it supports the biosphere of the surface (Singh and Preeti, 2017). This resource has been put under pressure by a fast-growing population that has increased and intensified its use for agricultural activities, industrialisation, mining and settlements (Halder et al., 2021; Nguyen et al., 2021; Talukdar et al., 2020; Amin and Fazal, 2012).

Projections of the world's population for 2050 indicate an increase of two billion people to almost 9.7 billion, with more than 50% of the world's growing population coming from sub-Saharan countries, which will double (Musetsho et al., 2021; Nations, n.d.). This fast-growing population will reshape land use and land cover (LULC), transforming it over time (Talukdar et al., 2020; Singh and Preeti, 2017).

As a consequence of this transformation, the interaction of the energy, water and carbon cycles between the land and atmosphere will be disrupted. This will disturb the ecological environment with impacts that go from increasing greenhouse emissions to soil degradation, affecting or being affected by the climate (Dissani et al., 2021; Tibebe et al., 2020).

Inspecting earth from space either by direct interpretation or mathematical modelling has proven to be an important mechanism for understanding the natural and anthropogenic processes affecting the biosphere and environment, providing time-to-time information with more precise and accurate results and giving a long-term view of their transformation and impacts (Singh et al., 2021; Tomaszewski et al., 2021).

Therefore, assessing and monitoring land use has been a major concern for the scientific community for the past century (Joshi et al., 2016). In recent decades, progress toward creating robust methods for monitoring land use/cover was achieved with the introduction of new remotely sensed data, machine learning and artificial intelligence approaches (Joshi et al., 2016).

A range of models and algorithms were developed and applied, with the common advantage of reducing computation time processing data, allowing big data analysis and assessing areas with irregular or complex relief for ground truth data collection (Carcausto et al., 2022; Wang et al., 2022; Nguyen et al., 2021). The evolution of Remote Sensing (RS) from optical to active radiometric instruments has increased the use of those models at local, regional and planetary scales (Calderón-Loor et al., 2021; Schulz et al., 2021).

However, few land assessments have been conducted in developing countries (Nguyen et al., 2021). Those conducted were under census surveys by government institutions, as independent bodies, covering large areas (national or regional scale). As such, the information was collected using laborious and traditional methods, with time and budget constraints and generally with different approaches and periods, not allowing the creation of a national geospatial database (Wang et al., 2022; Nguyen et al., 2021; Oliveira et al., 2019).

This research was undertaken in Boane, a southwest district of Maputo Province, Mozambique. This district has undergone widespread economic development and a fast-growing population, accounting for 5.22% increase in the last four decades (National Statistical Institute, n.d.), with information about land cover changes (extend, quantity, direction and trend), driving forces and impacts remaining unknown.

This was an attempt to demonstrate the value of earth observation data assessing changes in land use land cover over 40 years (1980 to 2020), through a supervised process on a Google Earth Engine (GEE) platform. A set of five Landsat images with ten-year intervals were analysed to extract and compare seven land classes, i.e., agriculture, forest, built-up, bare, rock, wetland and waterbody, using a random forest (RF) algorithm, and predict the future (2050) using CA-Markov model.

1.2. Problem Statement

According to Mozambique's national forestry inventory, native forests cover 43% of the territory, mainly the Miombo woodlands, which is rapidly depleting. From this, agriculture has been considered the main driver of land cover conversion, with 65% of the country's annual quota, followed by settlements at 12%, wood extraction at 8%, and wood fuel consumption at 7% (Aquino et al., 2018; FAO, 2020; MITADER, 2016). From census and projection reports (Table A.1, Figure A.1) by the National Statistical Institute, the population of Boane grew at an annual average rate of 4.57% over the last 40 years, accounting for a total increase of 205073 inhabitants (5.22%). By 2050, the population is expected to more than double, accounting for 328424 inhabitants (1.34%). In Mozambique, land is owned by the state, which recognises the right of land use (Land Act. Nr. 19/97), where transmission by good faith or customary occupations (traditional) are most common, followed by inheritance, state grant, purchase or lease (CCM, 2004; Todorovski et al., 2013). Generally, this transmission is led by local leaders either in rural or urban areas, creating an indiscriminate land occupation (Todorovski et al., 2013). As this occupation does not follow a formal zoning plan to allocate land to social or economic activities, such as infrastructures or settlements, it is overweighing the land capacity (Balas et al., 2021). Although Matule and Macarringue (2020), assessing soil loss and vulnerability in Boane District, Mozambique, identified 53.3% of the district as stable (with favourable or not vulnerable conditions), special attention be given to the fast-growing population rate, as well as the need to follow zoning plans, as crucial to maintain good practice and ensure sustainable land use. Since no assessment was carried out to analyse this massive and indiscriminate land occupation (Figure 1), which might have increased land transformation in Boane, this research attempted to map and quantify changes in LULC over time and predict future use scenarios. The findings will help the efforts to establish a development plan supported by evidence-based solutions, which can improve the design of sustainable environmental management strategies, good ecosystem and natural resource practices.

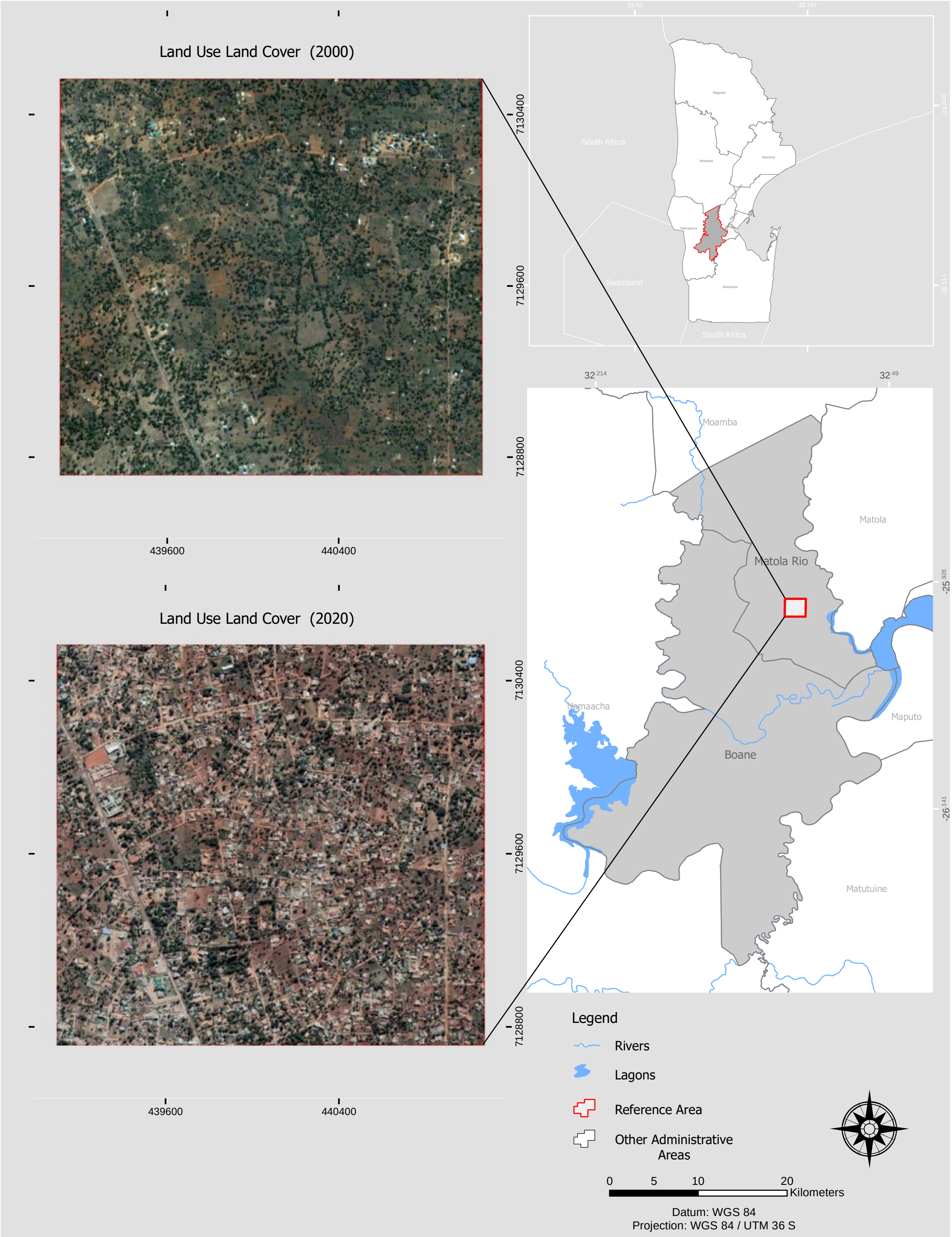

Figure 1. Land use land cover situation of Boane, between 2000 and 2020, using historical Google Earth images

1.3. Research Questions

a) How does LULC vary in extent and intensity over time and space in the study area?

b) What have been the key factors driving LULC transformation over the past 40 years?

c) How will maintaining the current patterns of LULC have a significant impact on the environment in the future?

1.4. Aim of the Study

This research aimed to demonstrate the value of earth observation data mapping the spatio-temporal dynamics of Boane, Mozambique, from 1980-2020. Using a random forest technique, seven categories of LULC were extracted and analysed from the Landsat images to identify and quantify natural and anthropogenic processes leading to land transformation and their impacts. The results were used to predict future land use scenarios for 30 years.

1.5. Objectives of the Research

To achieve the above aim, the following objectives were set:

a) Map LULC changes at ten-year intervals using Landsat data and random forest algorithm;

b) Quantify the directions and metrics of LULC change between classified images using a change detection technique;

c) Identify the natural and anthropogenic key factors shifting LULC changes;

d) Predict scenarios of future LULC transformation between 2020 and 2050 using the CA-MC model;

1.6. Outline of the Research

This research report comprises six chapters. The first chapter is the general introduction, providing the background that supports the research, the problem statement and research questions, aim and objectives of the research. The second chapter is the literature review, which discusses the relevant literature relating to the research topic and their main findings. The discussion begins with principles of land use land cover mapping, image classification, and change detection. This chapter ends with future prediction process and a broad overview of the conceptual approach of RS and fundamentals for data capture. The third chapter presents the material and methods used in this research, describing the study area, RS data acquisition, sampling collection, image classification, accuracy assessment and change detection techniques. This chapter ends with a description of the future prediction process. The fourth chapter presents the research outputs, outlining the statistics data of the mapping process, the algorithm performance and post-classification, giving a view of the dynamic of changes over time. This chapter ends with the results of future predictions for the next 30 years. The fifth chapter discusses the main findings of the results, analysing and comparing the results with those produced by other researchers. The last chapter (sixth) provides the study's conclusions, summarising the main findings and limitations of the research.

CHAPTER TWO

2. LITERATURE REVIEW

The early years of LULC analyses in Mozambique were more qualitative, describing general landscape characteristics based on community and stakeholder reports or witnesses. In later years, it became quantitative, with more comparative studies analysing LULC changes spatially and temporarily (Macarringue et al., 2020).

Since the independence of Mozambique (1975), several attempts to assess and monitor land use land cover were put in place mostly to estimate forest cover areas at the medium or large scale. Under the national forest inventories, those attempts have been taken successively from 1980, 1994, 1997, and recently in 2017, based on aerial photo interpretation of small plotted areas, controlled through extensive field works, and later with a visual interpretation of satellite images (Marzoli, n.d.; Mazalo, 2018; MITADER, 2018).

According to Macarringue et al. (2020) and Oliveira et al. (2019), as those surveys were undertaken in different periods and using different methodologies, they are difficult to compare and create a national spatial database. Hence, the first approach to harmonise procedures to classify LULC maps was through the Africover project under the Food and Agriculture Organization proposal, when several African countries adopted the revised land cover legend and classification (Mazalo, 2018).

Therefore, the first LULC reference maps (1997) were produced based on this approach and were used as comparative maps for many years by researchers assessing LULC (Mazalo, 2018). Among other attempts, Oliveira et al. (2019) considered the development of WebGIS Mozambique (2011) and Spatial Development Program (2016) platforms as the most relevant approaches, aiming to systematically collect, organise and publish spatial data, from both public and private sources. The availability of this geospatial data of the country to all stakeholders creates an environment that enables the development of applications and tools that have helped local communities and industries (Oliveira et al., 2019).

Despite the emergence and availability of earth observation data, the issue of monitoring changes in LULC over time has increased. Several other researchers and studies have been conducted recently using the most advanced techniques in RS and geographic information systems, mostly assessing changes in LULC, forest cover, mangrove, soil loss and deforestation at local, regional or national scales.

2.1 Land Use Land Cover Mapping

As the main scheme to classify land use in official surveys of Mozambique, the land cover classification system was adopted from the Food and Agriculture Organization, which has three hierarchy groups of distinction (Jansen & Di Gregorio, 2000; Mazalo, 2018) . The first (initial), with two levels, represents the most aggregated classification group used for regional and other large-scale applications. Within each initial level of distinction, there are two more detailed LULC classes (second), which comprise four levels of distinction, each deriving the third group with eight levels of distinction (Jansen & Di Gregorio, 2000).

Land classification schemes typically address both LULC, as they are terminologies used to characterise the state of the earth's landscape, either due to natural or anthropogenic action (LaGro, 2005; Yadav et al., 2019). As of, land cover is associated with physical material observed on the earth's surface and is usually used to describe the biophysical characteristics, including vegetation, water, soil, rocks and other physical aspects (Yadav et al., 2019; Singh and Preeti, 2017).

Changes in land cover can be in the form of conversion when the land cover completely changes from one type to another or by modification in which there is a subtle change, but the property of the class is maintained (Joshi et al., 2016). On the other hand, land use depends on how land has been modified by anthropogenic activities, which can be roads, buildings and other constructed elements usually associated with economic purposes (Yadav et al., 2019). Land uses can be changed by adopting, through expansion or by changing the management system within a land use class (Joshi et al., 2016).

For instance, Dias (2015), compared Spot 4 images of Marracuene district with the Mozambican reference map, which used the land cover classification system approach used by Food and Agriculture Organization, assessed changes in LULC. Likewise, Mazalo (2018) compared with Landsat 5 when mapping land occupation in the same district. Manteigas (2009), through overlapping the reference map with Landsat 5 images, assessed the potential of satellite images monitoring LULC in the Maganja da Costa district.

Additionally, other researchers successfully mapped LULC changes, using the most recent technics in earth observation and geographic information systems, which do not rely on reference maps. Matule and Macarringue (2020), using Landsat 8, ASTER and GDTM V2 images, assessed the soil vulnerability of Boane. Oliveira et al. (2019), using Landsat 8 within the GEE platform, mapped LULC on a large scale (Mozambique). Macaringue (2022), using the same type of images and platforms, regionally mapped the northern region of Mozambique.

2.2 Image Classification and Machine Learning Algorithms

There was always a link between progress in RS and the need for improved classification algorithms to address the massive data produced. Hence, from aerial photo interpretation to machine learning algorithms there was a giant step in the image classification process (Halder et al., 2021; Majumdar, 2020; Amin and Fazal, 2012).

One of the main objectives of classifying images is to transform data within pixel values (captured by the RS process) into thematic information, which can be useful to assess changes or dynamics on the earth's surface (Yadav et al., 2019). In recent decades, a number of parametric and non-parametric algorithms, such as bayes, k-means, maximum likelihood, random forest, support vector machine, artificial neural network, were developed (Wang et al., 2021; Joshi et al. 2016). There was a transition from the classic and traditional methods which require that data does not significantly deviate from the normal distribution curve, to non-parametric machine learning algorithms, improving the precision and accuracy of image classification processes (Wang et al., 2021; Joshi et al. 2016).

In this regard, Tuzine (2011), mapped LULC in the forest of Inhamacari, Manica District, Mozambique, using Ikono II images and Fuzzy algorithm, and obtained a 55.5% accuracy assessment and a kappa coefficient of 0.46. Soares (n.d.), assessed the relationship between forest burning action and changes in LULC, using the maximum likelihood algorithm, reached values of accuracy between 78% to 80%. Furthermore, Oliveira et al. (2019), using the RF algorithm in the GEE platform, reached 76.23% accuracy. Similarly, Macarringue (2022) achieved 80.93% accuracy and a kappa coefficient of 88.08% when mapping at national and regional scales, respectively.

In Africa, Gudo et al. (2022) analysed the spatio-temporal dynamics of LULC changes in South Sudan, with an average overall accuracy of 97.15 and a kappa coefficient of 0.954. Nakamo et al. (2022) assessed land cover changes in Tanzania with 97.16% accuracy and a 0.9547 kappa coefficient, Schulz et al. (2021) mapped land use in a heterogeneous landscape in Niger with 72% accuracy, and Zvobgo and Tsoka (2021) assessed causes of the deforestation rate in Zimbabwe, with 91.25% accuracy and a 0.89 kappa coefficient. These studies used the RF algorithm in a GEE environment, producing highly accurate land use maps, compared to other researchers who used different classifier algorithms.

Although factors such as RS data quality, the selection of a precise classification process and some sort of producer expertise was listed as the main drawback of the image classification process (Rwanga and Ndambuki, 2017). Other major drawbacks classifying images in Mozambique, and other African countries, are some characteristics of most settlements areas, which are rural and informal with few or non-zoning plans, house roofs mainly of straw, grass, sticks and stakes, as well as the rainfed agriculture practised by a majority of households, which is mostly with vegetation removal or non-concentrated cultures (Macarringue et al., 2020).

These physical aspects affect the identification of feature objects in earth observation data with medium resolution that are freely available and most used in developing countries, such as Mozambique, leading to the misclassification of images either as barren lands, rock areas or forest areas (savannas) (Macarringue et al., 2020).

2.3 Change Detection and Land Transformation

The fundamental idea behind change detection is to evaluate the state of land features, through image comparisons, at different time-steps (Lu et al., 2004). In this process, one is interested in identifying differences in the extent of observed landscape in time and attributing those changes to a specific cause (Kesgin and Nurlu, 2008; Zvobgo and Tsoka, 2021).

In change detection, the classification process is considered effective and precise as it specifies the magnitude of changes, rate of change and direction of change, as the analysis is performed through a pixel-by-pixel comparison (Bagarinao et al., 2020; Goswami et al., 2022; Lu et al., 2004). The ability to observe changes through classified images allows us to determine whether a land class has expanded their areal extent (increase) or reduced (decrease), or either way, it remains the same (Lu et al., 2004).

From this statement, it can be assumed that a land class can change from one type to another, go through structural changes without changing its type, or even remain in the same state (Singh and Preeti, 2017). Therefore, change detection is mostly used as a statistical tool to identify, quantify and explain the amount of change in LULC.

In their studies, Goswami et al. (2022), comparing algebraic and machine learning methods, Thakkar et al. (2017) and Zaitunah et al. (2022), improving the classification of LULC mapping land cover and vegetation, Jombo et al. (2017), quantifying landscape transformation, Kesgin and Nurlu (2008), assessing land cover changes on the coastal zone, Hassan et al. (2016), assessing the dynamics of LULC change, and Amin and Fazal (2012), assessing land transformation, all used change detection as a post-classification method.

For example, Nkundabose et al. (2021), assessing LULC in a rural region of Eastern Province in Rwanda, applied RS and geographic information systems to compare two images of the same scene, taken at different moments to identify their differences. They obtained satisfactory information about land transformation and recommended that other researchers include socio-ecological analysis and other surveys to better understand the drivers for the land cover changes.

Amin and Fazal (2012), analysing land transformation in urban areas in Srinagar, India, combined the use of RS data and geographic information systems through a change detection method, enabled them to estimate the nature, extent and rate of LULC transformation. As a result, they witnessed rapid and large-scale LULC changes and transformation. The increasing urban population and socio-economic transformation were identified as driving forces of change.

Change detection provides an understanding of all the dynamics involved in the relationship between natural phenomena and human actions. Among other factors, topography conditions, droughts, floods, soil erosion and other natural phenomena (biophysics), or deforestation, urbanisation, demographics, social and economic conditions (anthropologic) have been seen as the main driving force for land transformation.

2.4 Land Use Land Cover Future Prediction

In recent years, it has become common to monitor and forecast future LULC patterns using simulation and prediction models (Aburas et al., 2016). Hence, a variety of models have been developed, including but not limited to the traditional CA, which is based on dynamic assessments of LULC, and those relying on quantitative data such as MC, Logistic Regression, evolutionary artificial neural networks and agent-based models, each with an acceptable level of accuracy (Hua, 2017; Subedi, 2013).

For example, as part of their LULC studies, Aburas et al. (2017) integrated Analytic Hierarchy Process and Frequency Ratios based on the CA-MC modelling urban growth, Tariq et al. (2022), Mishra et al. (2014) and Kesgin and Nurlu (2008), used Land Change Modeler (LCM) and CA-MC assessing and predicting urban growth, Asadi et al. (2022) compared the accuracy of ANN and CA-MC simulating urban sprawly, Gharaibeh et al. (2020) improved LULC modelling using ANN and CA-MC, Nugroho et al. (2018) used ANN modelling urban growth, Alshari and Gawali (2022) and Muhammad et al., (2022) used Molusce modelling for LULC change; all successfully predicted the future of LULC.

Among these models, the CA model was mostly used and one of the most reliable for simulation and prediction. In addition to being easy to use, this model can simulate any complex pattern, has an open structure, is easily integrated with other models, and can simulate both spatial and temporal patterns (Aburas et al., 2021; Aburas et al., 2016). The drawback of the model is the lack of producing quantity data, and it is difficult to include physical and socio-economic driving forces (Aburas et al., 2021; Al-sharif and Pradhan, 2013).

To overcome this issue, this model has been integrated with a quantitative and spatio-temporal model, such as MC or combined with others, such as the Analytic Hierarchy Process and Logistic Regression, to achieve accurate and realistic results (Aburas et al., 2016). By combining with the MC model, the CA model adds spatial proximity and spectral distribution to the observed elements, and, using the probability areas created by MC, can forecast LULC spatial distribution over time (Asadi *et al.*, 2022; Aburas *et al.*, 2016).

This hybrid model was successfully used by Merhej et al. (2022) to predict LULC changes. Gemmechis (2022) and Azizi et al. (2016), assessing LULC spatio-temporal dynamics, Aburas et al. (2016; 2021) and Al-Khaqani and Al (2022), simulating and predicting urban expansion, Liping et al. (2018), Hua (2017) and Al-sharif and Pradhan (2013), monitoring and predicting LULC changes, all achieved high Kappa Index of Agreement.

CA-MC models have the advantage of not requiring rich data, as they can forecast using only historical data (at least two periods' images). Notwithstanding, other factors, such as slope, aspect, population density and distance to facilities, can be considered (Aburas *et al.*, 2021). Although this model doesn't analyse or explain the driving forces of LULC change, it can play a significant role in processes of policy-making, land use planning and natural resource management, as it produces robust, reasonable and accurate results (Aburas et al., 2016).

2.5 Concept and Data Capture in Remote Sensing

By combining a systematic and scientific approach of analysis and investigation, RS produces useful information in the hopes of solving past, current or future problems (Bhatta, 2013). The rationale behind using RS data is to reduce the costs and time associated with field data collection, mostly used in traditional campaigns assessing and processing the earth's surface information (Shahtahmassebi, 2021).

For decades, events affecting the earth's ecosystem have been a concern for planners, ecologists and researchers (Joshi et al., 2016). Since then, the development of precise and accurate RS tools has led to the provision of reliable, powerful and valuable information about natural conditions, allowing us to assess and monitor their temporal dynamics (Hassan et al., 2016).

Hence, there are a large number of RS sources of information (Sentinel, Landsat, Radarsat, ASTER, STRM, MODIS, TRMM, etc.), and each has its own use with a set of strengths and weaknesses (Schulz et al., 2021). For example, Chen et al. (2021), Cissell et al. (2021), Schulz et al. (2021) and Nguyen et al. (2021) used Sentinel 1 and Sentinel 2 to assess and map mangrove cover, maize area, LULC, and monitor the environment, respectively.

On the other hand, Nkundabose et al. (2021) and Bagarinao et al. (2020) used Landsat images to map LULC. Kusiima et al. (2022), Thiam et al. (2021), Gaur et al. (2020) and Tibebe et al. (2020), monitoring land cover spacio-temporal dynamic of changes, Yesuph and Dagnew (2019), Asadi et al. (2022), Halder et al. (2021) and Dessu et al. (2020), assessing urban expansion or sprawling, and Singh and Preeti (2017), assessing land transformation, all achieved very accurate results.

In Mozambique, Ameja et al. (2022), Macarringue et al. (2020, 2019, 2022), Mazalo (2018), Mucova et al. (2018) and Tuzine (2011), combined the use of Landsat with Sentinel collection to assess land transformation mostly in protected areas (national parks and reserves), monitor forest cover, soil qualities, always associated with relevant field work to better understand their driving forces and propose sustainable use planning.

One of the main shortcomings in data produced by RS instruments is quality, which is greatly determined by the sensor's parameters. According to Schulz et al. (2021), when there is an improvement in one resolution parameter, either radiometric, spectral, spatial or temporal, it is reflected in another, thus, affecting the images' quality.

The phenological characteristics of vegetation cover, soil moisture, cloud cover or atmospheric conditions are another drawback associated with using RS data. Most optical sensors, including Landsat, are impacted by these conditions, particularly weather conditions in tropical areas (Tomaszewski et al., 2021).

.

CHAPTER THREE

3. RESEARCH METHOD AND MATERIALS

3.1 Study Area

The study area (Figure 2) is spread over Boane District in the southwestern part of Maputo Province, Mozambique, between 32°20′ E and 26°22′ S. This area lies between Maputo city, Matutuine, Namaacha, Moamba and Matola districts, covering a total area of 820 square kilometres (Sq.km) within an altitude of 200 to 1 metre (m) above the sea level.

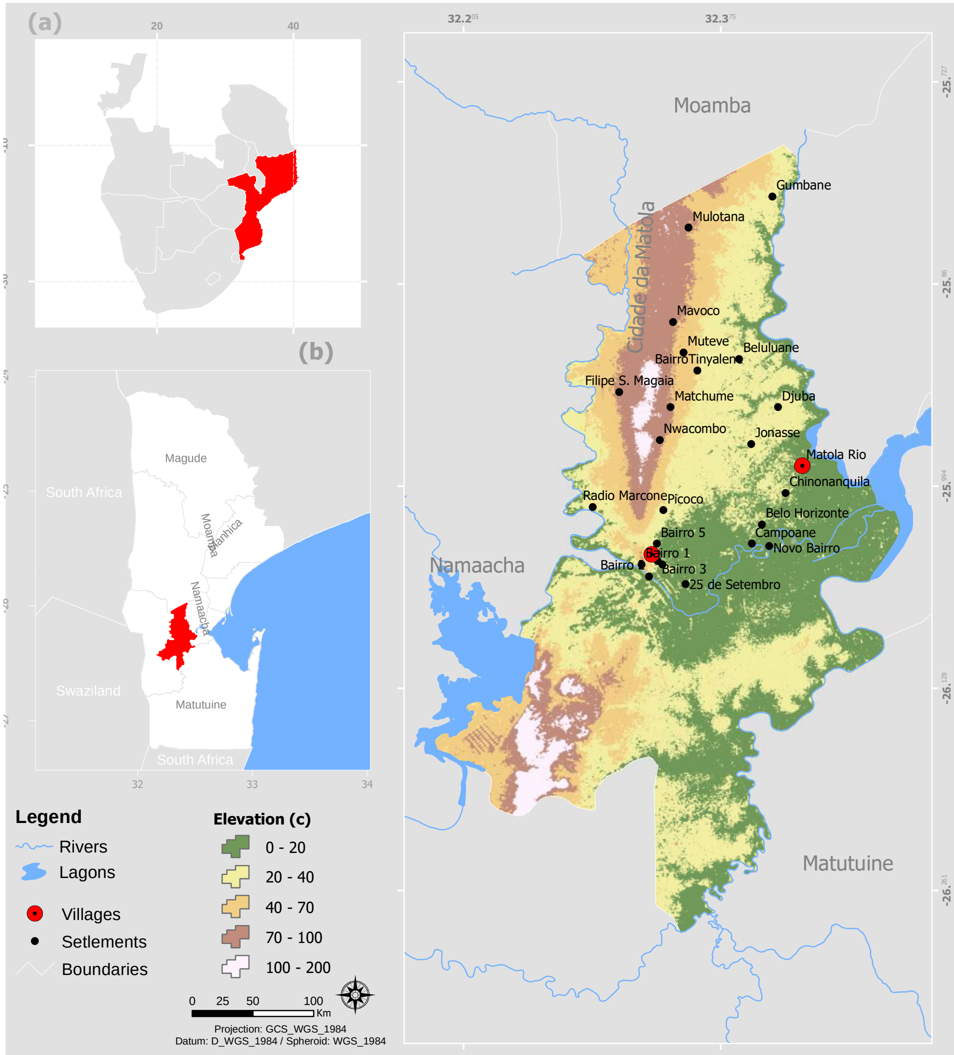

Figure 2. Geographic location of the study area, its (a) regional and (b) national location, and (c) height values extracted from the advanced spaceborne thermal emission and reflection radiometer sensor data

It consists of two major administrative areas, Boane and Matola Rio, at south and north, respectively (State Administration Ministry, n.d). The relief is marked by highlands crossing from north to south as part of the Lebombo mountains, the borderline with the Namaacha district, and an altitude ranging from 200 to 250 m. A transition area from medium to lowlands is observed from west to east until the coastline, with an altitude of 200 to 1 m (Macarringue et al., 2019).

Geologically, it is mainly composed of basalt and rhyolites from volcanic rocks of the Jurassic age and eluvial floodplain clay sands from a more recent age (Matule and Macarringue, 2020). The vegetation consists of extensive savannahs and a mosaic of pastures and forests of mountain areas (MITADER, 2016). The rainfall regime is unimodal, with one peak of the wet season observed between November and March and another peak of a dry season between April to October (Herrmann and Mohr, 2011). The annual average precipitation is 752 mm, strongly affected by the intertropical convergence, which modifies the climate (Herrmann and Mohr, 2011).

3.2 Data Acquisition and Processing

3.2.1 Remote Sensing Data

To map and quantify the spatio-temporal dynamics of LULC between 1980 and 2020, a set of five Landsat images (Table 1) from the thematic mapper (TM) sensor for the years 1984, 1990 and 2000, enhanced thematic mapper plus (ETM+) for 2010, and operational land imager and thermal infrared sensor (OLI/TIRS) for 2020, was freely downloaded from the United States Geological Survey (USGS.gov | Science for a changing world), using GEE.

This research used the Landsat collection because of the long duration of data collection (over 50 years), good multispectral and spatial resolution (15 to 30 m), real-time resolution of 16 repeated cycle days, freely available and the most used for scientific research purposes (Jombo et al., 2017). The images were selected based on the cloud cover condition (less than 10% cloud cover) using a temporal filter between January to December of each reference year, and clipped with the area of interest (study area) boundaries mask.

To avoid differences in pixel size between images, a float function was applied to give the same pixel size as the OLI sensor (30 m). All images were then converted to 32 bits to be exported from GEE and used in the ArcGIS 10.2 environment. In GEE, all critical but time-consuming satellite image processing operations, such as radiometric and geometric corrections, mosaicking, stacking and cloud cover filtering, was performed quickly , as the data are in a ready-to-use format (Bhatta, 2013; Lefulebe et al., 2022; Nguyen et al., 2021).By integrating robust data processing and analysis techniques, this platform enables users to access, manipulate and analyses massive spatial data from multiple sources (Bhatta, 2013; Ghosh et al., 2022; Nguyen et al., 2021).

Other remotely sensing data from the advanced spaceborne thermal emission and reflection radiometer (ASTER) sensor, downloaded from Earth Explorer (EE), a USGS web page, were used to extract the elevation values using the digital elevation model (DEM).

Table 1. Detailed characteristics of earth observation data, extracted from Landsat thematic mapper, enhanced thematic mapper plus and operational land imager and thermal infrared sensors

Year	Path	Row	Spatial Resolution	Sensor	Date Acquired
2020	167	78	30m	OLI-TIRS	06 07 2020
2010	168	78	30m	ETM+	08 06 2010
2000	167	78	30m	TM	01 09 2000
1990	168	78	30m	TM	09 06 1990
1984	167	78	30m	TM	01 06 1984

3.2.2 Land Use Land Cover Mapping

To map LULC, seven classes (Table 2) representing features of interest, were adopted by adapting the third group of land cover classification system from the Food and Agriculture Organization, and used in official surveys in Mozambique, as the most desegregated, i.e., agriculture, forest, build-up, barren lands, rock areas, wetlands and water bodies (Jansen & Di Gregorio, 2000).

These classes were identified and differentiated using spectral signatures, tone, texture and pattern through on-screen digitalisation (Digra et al., 2022; Gilani et al., 2021).Therefore, agricultural class integrated in cultivated and managed terrestrial areas level, and artificial cover subgroup (primarily vegetated terrestrial group) was considered vegetation that is planted or cultivated with an intent to harvest, where the natural vegetation has been removed or modified and replaced by other types of vegetative cover of anthropogenic origin. This vegetation is artificial and requires human activities to maintain in the long term (Jansen & Di Gregorio, 2000). Forest, in the natural and semi-natural vegetation level, and artificial cover subgroup (primarily vegetated terrestrial) was considered areas where the vegetative cover is in balance with the abiotic and biotic forces of its biotope. This class can include semi-natural vegetation, which is vegetation not planted by humans but influenced by human actions (Jansen & Di Gregorio, 2000).

Wetlands, within the natural and semi-natural aquatic or regularly flooded vegetation level, in aquatic or regularly flooded subgroup (primarily vegetated) describes areas that are transitional between pure terrestrial and aquatic systems and where the water table is usually at or near the surface, or the land is covered by shallow water (Jansen & Di Gregorio, 2000). The class of waterbodies, under natural and artificial waterbodies, snow and ice level, in the aquatic or regularly flooded subgroup (primarily non-vegetated) refers to areas that are naturally covered by water or due to the construction of artefacts (Jansen & Di Gregorio, 2000).

Build-up, integrated into the artificial surfaces and associated areas level, artificial cover subgroup (primarily non-vegetated terrestrial), was considered areas that have an artificial cover as a result of human activities, such as construction, extraction or waste disposal (Jansen & Di Gregorio, 2000). Bare lands, under the bare areas level, artificial cover subgroup (primarily non-vegetated terrestrial), describes areas that do not have an artificial cover as a result of human activities. These include areas with less than 4% vegetative cover, bare rock areas, sands and deserts. As the rocks class is included in the category of bare lands, all characteristics are similar (Jansen & Di Gregorio, 2000).

Table 2. Distinction at the third level of the Dichotomous Phase into seven major land cover types

Land use land cover class	Description
Agriculture	wheat fields, orchards, rubber and teak plantations
Forest	extended vegetation areas, natural grown trees, grass, pasture

Land use land cover class	Description
Build-up	cities, towns, transportation, extraction (open mines and quarries) or waste disposal
Barren	sands and deserts
Rock	bare rock areas
Wetlands	mangroves, marshes, swamps, bogs or flats
Water	lakes, rivers, snow or ice, reservoirs, canals, artificial lakes

3.2.3 Training and Validation Sample Data

According to Tempfli et al. (2009), as strategy for sampling in LULC, it is recommended to use simple random sample or stratified random sample methods. In simple random sample, all training data are selected randomly with an equal probability of being selected but independent from each other, with no restriction on randomisation (Gonçalves and Assis, 2007; Tempfli et al., 2009).

In stratified random sampling, the study area is divided into strata (sub-areas) where the simple random sample is applied in each stratum, with the sample size and restriction on randomisation known (Gudo et al. 2022; Gonçalves and Assis, 2007; Tempfli et al., 2009). This research used stratified random sampling.

Nguyen et al. (2021) recommend 50 samples per class when dealing with areas that are less than 4 000 Sq.km or when there are fewer than 12 categories. Therefore, 1667 features (Table 3) representing all seven classes were collected, from which 1243 (75%) were used to train the algorithm to learn how to perform the correspondence between each pixel value with their class and classify images using a decision tree, and 424 (25%) were used as validation data (Nguyen et al., 2021; Chakraborty et al., 2013).

It should be noted that each sample features were derived from visual interpretations of Landsat images at medium resolution (30m) and corrected using historic high resolution (0.52m) google earth images. According to Gao & Song, (2022), Roy et al. (2010) and Puig et al. (2002), using this approach, better results are obtained as one refines the other, correcting errors.

The universe was divided into mutually exclusive and non-overlapping classes to produce separate and evenly distributed estimations, to increase the precision of the class representativeness (Gonçalves and Assis, 2007; Tempfli et al., 2009).

Table 3. Total number of sample feature collected per land class, for training and validation data in each reference year

Land use land cover class	Feature Collected					
	1984	1990	2000	2010	2020	Subtotal 2
Agriculture	34	46	50	47	54	231
Forest	50	50	46	45	42	233
Build-up	31	51	72	60	52	266
Barren	34	50	50	49	50	233
Rock	37	50	45	35	51	218
Wetland	50	50	50	44	42	236
Water	50	50	50	49	51	250
Subtotal 1	286	347	363	329	342	1667
Training Data	200	274	277	241	251	1243
Validation Data	86	73	86	88	91	424

3.2.4 Image Classification and Algorithm Selected

Through a digital image classification process, all reference images were classified based on the texture and spectral signature of the feature objects in a supervised classification process applying the RF algorithm (Puig et al., 2002). This ensemble learning technique (RF) is a non-parametric algorithm with multiple decision trees that randomly and systematically label features from training data and conduct cross-validation of information (Calderón-Loor et al., 2021; Chen et al., 2021; Jhonnerie et al., 2015).

As part of this integrated algorithm, two-thirds of the samples are used for training (bag samples), one-third is used for internal cross-validation (out-of-bag samples) and bootstrap samples are used to predict, generating independent training sets in which features are randomly selected from a decision tree by averaging or voting between the trees' predictions (Calderón-Loor et al., 2021; Chen et al., 2021; Nguyen et al., 2021).

To improve the overall performance of the ensembled algorithms, different hyperparameters controlling the structure of the forest, each individual tree and the randomness, i.e., number of trees, variables Per Split, min Leaf Population, bag Fraction, max Nodes and seed, must be set (tuned) before running the model (Probst et al., 2019).

As recommended by Nguyen et al. (2021) and Bayas et al. (2022), in RF at least two tuning parameters are required for each sample, i.e., the number of trees (n-tree), which is defined by the user, and the number of features considered for each tree when splitting a node (m-tree) (Obaid et al., 2023).

Similar to other ensembled machine learning tuning, the remain hyperparameters in RF are optional for the users as it was end-built-designed to produce good results with default values, working perfectly to predict (Amusa et al., 2021; Bilolikar et al., 2023; Probst et al., 2019). The challenge in choosing the optimal hyperparameters in most ensemble machine learning is the availability of different spatial resolution remotely sensing data, as they have different responses when calibrating a model (Song et al., 2018; Shao et al., 2012).

RF optimises the classification results and selects informative variables but doesn't consider the correlation among variables to quantify their importance (Song et al., 2018). This algorithm (RF) is widely used because it calculates and overcomes data disturbances in a multi-dimensional dataset (Nakamo et al., 2022).

In this research, 200 trees and 1667 feature points were used to train the algorithm and improve the correctness of the image classification. The remaining hyperparameter was used as the algorithm's default values (Probst et al., 2019).

3.2.5 Accuracy Assessment

Accuracy assessment is a statistical tool mostly used to validate the results of image classification (Chughtai et al. 2021). It expresses the quality of the classification as it compares the results and reference data (Nguyen et al., 2021). The correctness of image classification is obtained by assessing if the number of errors generated by the classifier algorithm is between the expected confidence interval compared with another batch of samples collected as reference or ground truth data (Nguyen et al., 2021; Jasim et al., 2016).

Among others, the confusion matrix or error matrix is the most common method to validate the results of RS data, as it provides complete information by computing changes that occurred pixel-by-pixel, considered the most precise procedure in an accuracy assessment (Chughtai et al., 2021; Meli Fokeng et al., 2020).

The main accuracy coefficients estimated from the confusion matrix were overall accuracy and the kappa coefficient. (Meli Fokeng et al., 2020). Overall accuracy indicates the proportion of reference sites correctly mapped. This is expressed as a percentage, with 100% being a perfect classification and 0% the worst classification (Meli Fokeng et al., 2020). Overall accuracy is calculated by adding the number of correctly classified sites (values in the diagonal line) and dividing by the total number of reference sites (Bhatta, 2013; Meli Fokeng et al., 2020).

The kappa coefficient (Equation 1) is a statistical test used to measure the straightness between the model used to predict the image classification, i.e., it evaluates how well the classification was performed compared to just randomly assigning values (Meli Fokeng et al., 2020; Bhatta, 2013).

$$Kappa = \frac{\mathrm{N}\sum_{i=1^*}^{r} X_{ii} - \sum_{i=1^*}^{r}(X_{i+} + X_{+i})}{N^2 - \sum_{i=1^*}^{r}(X_{i+} + X_{+i})} \qquad \text{(Equation 1)}$$

Where:

N is the total number of sites in the matrix; R is the number of rows; X_{ii} is the number in row i and column I; X_{+i} is the total for row I, and X_{i+} is the total for column L.

The kappa coefficient is represented in a scale range of 0 to 1 (Table 4), where zero indicates that the classification was randomly classified, and one indicates perfect agreement between the ground truth data and the image classified (Meli Fokeng et al., 2020; Bhatta, 2013). Omission error, commission error, producer accuracy and user accuracy are other important parameters that can be extracted from the confusion matrix, which can explain and sustain analyses if the data were correctly classified or not (Meli Fokeng et al., 2020).

Omission error, usually referred to as *Type I error,* is the number of reference data omitted or left out from the correct class during the classification process, while the error of commission indicates how many sites were incorrectly classified in the class (Meli Fokeng et al., 2020). User accuracy, referred to as *reliability*, represents the accuracy viewed by the map user, expressing how often the class on the map will be presented in the ground truth data, and producer accuracy, which is the accuracy viewed by the map producer, indicates how often the real features on the ground are correctly represented on the classified map (Meli Fokeng et al., 2020).

Table 4. Kappa coefficient values indicating the degree of agreement between the model and classification process

Kappa Value	Straightness Agreement
<0,20	Poor
0.21 - 0.40	Fair
0.41 - 0.60	Moderate
0.61 - 0.80	Good
0.81 - 1.00	Very good

3.2.6 Change Detection Analyse

According to Lu et al. (2004), to get good results when performing change detection, it should provide information on area changed, i.e., the magnitude of change (Equation 2) from which the percentage of change (Equation 3) and rate of change (Equation 4) are derived. The magnitude of change indicates the degree of expansion or contraction in the size of a land use class, where negative values represent a decrease in class size and positive values an increase (Goswami et al., 2022; Gudo et al., 2022; Bagarinao et al., 2020; Yesuph and Dagnew, 2019).

$$A = C - B \qquad \text{(Equation 2)}$$

$$K = \frac{C - B}{B} * 100 \qquad \text{(Equation 3)}$$

$$R = \frac{C - B}{D} \qquad \text{(Equation 4)}$$

Where:

(A) is the amplitude of change; (C) is the represent area of the final image; (B) represents the area of the initial image; (K) is the percentage of change in a class; (R) is the rate of change; and (D) is the time interval (Yesuph and Dagnew, 2019)

Other important measurements can be computed from change detection, such as persistence, gain and loss, total change, swapping and absolute net change, which helps to give the direction of change of each land cover class (Ameja et al., 2022; Gudo et al., 2022; Dessu et al., 2020; Gaur et al., 2020; Yesuph and Dagnew, 2019).

As a result of the change-detection analysis, a matrix (from – to) is generated where the values on the diagonal line indicate the unchanged pixels (areas), which is the persistence. Gains represent the difference between the total column class and persistence, while loss is the total row and persistence. Total change is a sum of gain and loss, and swapping is the difference between total change and net change. The difference between the percentages of change on the final image and the initial image is the net change (Dessu et al., 2020; Yesuph and Dagnew, 2019).

3.2.7 Population Growth and Land Transformation

To understand the population dynamic throughout the study period, a set of demographic indicators (Table A.1, Figure A.1) was calculated. By adapting Chel (2023), Calka et al. (2022) and Behera et al. (2018), the annual growth rate (Equation 5) was calculated and used to quantify the average number of persons per 100 inhabitants that annually changed between intercensal intervals. The net increase (Equation 6) was calculated as the absolute population change between two measured periods, while the growth percentage (Equation 7) was the relative population change. Other indicators were the annual increase (Equation 8), representing the number of inhabitants per year, and density (Equation 9), derived by division of the population with the district area in a masked file, and used as the number of inhabitants per spatial unit.

$$(R) = (ln\left(\frac{\mathrm{Pn+1}}{(\mathrm{Pn})}\right))/\mathrm{T} \qquad \text{(Equation 5)}$$

$$(Ni) = (\mathrm{Pn} + 1) - (\mathrm{Pn}) \qquad \text{(Equation 6)}$$

$$(P) = \frac{(\mathrm{Pn}+1)-\mathrm{Pn}}{\mathrm{Pn}} \qquad \text{(Equation 7)}$$

$$(Ai) = \frac{(\mathrm{Pn}+1)}{\mathrm{T}} \qquad \text{(Equation 8)}$$

$$(D) = \frac{(\mathrm{Pn}+1)}{\mathrm{S}} \qquad \text{(Equation 9)}$$

Where:

(R) is the annual growth rate, (P_{n+1}) is the population in the final year, (P_n) is the population in a previous year, (T) is the number of years between two measured periods, (Ni) is the net increase, (P) is the percentage of growth, (Ai) is the annual increase, (D) is the population density, and (S) is the study area surface.

As the anthropogenic actions dominate land transformation, a correlation analysis was performed using a Person's test (Equation 10) and simple linear regression analysis (Equation 11), using a data analysis tool and scatter plot in Microsoft Excel (Land et al., 2023; Kafy et al., 2021). The main objective performing correlation and regression analysis was to evaluate the relationship between a fast-growing population with changes in LULC and to test how this relationship is statistically significant for the overall changes observed (Tran et al., 2017). This will address the issue of identify the natural and anthropogenic factors shifting LULC.

The correlation values indicate that two variables are strongly correlated when they are very close to positive one (+1), which is a perfect positive correlation, i.e., increasing one variable will increase the other (Land et al., 2023; Tibebe et al., 2020). Contrarily, when the values are close to negative one (-1), there is a strong negative correlation between the variables, i.e., increasing one variable will decrease the other. For values near zero (0), either positive or negative will indicate a weak or no correlation between the variables, i.e., one variable cannot explain the other (Land et al., 2023; Tibebe et al., 2020).

The regression analysis indicates the statistical significance of the correlation (Land et al., 2023; Tibebe et al., 2020). These statistical tools (correlation and regression) are widely used to measure the correlation between two variables and to determine how changes in one variable might affect another (Land et al., 2023; Tibebe et al., 2020; Tran et al., 2017; Bernales et al., 2016).

$$\rho\ (x, y) = \frac{\text{Cov (x,y)}}{\sigma y * \sigma x} \quad \text{(Equation 10)}$$

$$Y = a + bx + \varepsilon \quad \text{(Equation 11)}$$

Where:

(ρ) is the correlation, (Cov) is the covariance, (σ) is the standard deviation, (y) is the dependent variable, (a) is the intercept, (b) is the slope, (x) is the independent variable, and (ε) is the error

These tools have been extensively used to measure the correlation between population and the increase of land surface temperature, increase of urban hit island and other purposes (Bernales et al., 2016; Kafy et al., 2021; Sarkar & Patra, 2022; Tran et al., 2017).

3.2.8 Land Use Land Cover Future Prediction

The future of LULC was predicted using CA-MC, which is a hybrid method that combines MC and CA models, in TerrSet software (Asadi et al., 2022). To forecast, the MC model produces a quantitative prediction incorporating the spatio-temporal dynamic created by the CA model, therefore, CA-MC is an integrated method, where one model complements the issue of another (Al-Khaqani and Al, 2022; Aburas et al., 2021; Aburas et al., 2016).

The MC process is ruled by random distribution probability, i.e., is stochastic and discrete in both, time and state (Gemmechis, 2022; Liping et al., 2018; Azizi et al., 2016). This model quantitatively predicts the future state of an event according to the state of one current or past event through a transition probability, giving a temporal dynamic (Al-Khaqani and Al, 2022; Gemmechis, 2022; Liu and Zhang, 2022; Tariq et al., 2022).

The model computes the transition likelihood (Equation 12) of two qualitative LULC images taken at different periods, (t) and (t+1), and evaluates quantitatively the change dynamics and temporal variation, producing a matrix of areas with a probability of change (P_{ij}) (Equations 13 and 14), without considering all the event history (Al-Khaqani and Al, 2022; Azizi et al., 2016).

$$S\ (t+1) = P_{ij} * S(t) \quad \text{(Equation 12)}$$

$$P_{ij} = \begin{bmatrix} P11 & P12 & Pn1 \\ P21 & P22 & Pn2 \\ Pn1 & Pn2 & Pnn \end{bmatrix} \qquad \text{(Equation 13)}$$

$$\left(0 < P_{ij} < 1 \text{ and } \sum_{i=1}^{n} \text{Pij} = 1, (\text{i}, \text{j} = 1,2, \dots \text{n})\right) \qquad \text{(Equation 14)}$$

Where:

S represents the states of the system, (t) is the time instant, (t + 1) is the coming future time instant, (P_{ij}) is the matrix of transition probability in a state.

By cross-tabulation, two products are generated, the transition areas, which are the number of pixels that are expected to change over a specific number of units predetermined (years), and the transition probability, which is the probability that each state will change to every other state (Tariq et al., 2022). From the matrices, the row refers to the LULC status and the transferring out situation on the initial state (t1), while columns are the status and transferring out situation on the end state (t+1) (Merhej et al., 2022).

Whereas, the CA model (Equation 15) adds the spatial proximity and spectral distribution to the observed elements, using the probability areas created by the MC model to forecast LULC spatial distribution over time (Aburas *et al.*, 2016; Asadi *et al.*, 2022).

$$S\ (t, t+1)\ f\ (S\ (t), N) \qquad \text{(Equation 15)}$$

Where:

(S) represents the states of discrete cells, (t)is the time instant, (t + 1) is the coming future time instant, (N) is the cellular field, and (f) is the transition rule of cellular states in the local space.

Therefore, through n-step in the CA-MC model, an output file (matrix) of transition and probability change between 2020 and 2050 were generated to simulate LULC prediction over 30 years (2050). As input data, a classified image of 2010 and another of 2020 were used as earlier (t) and later images (t+1), respectively. The gap period between them (10 years) was used as the time period, while the forecast period (30 years) was used as the time period to project (Gemmechis, 2022).

To keep the background areas of the images as they are, they were given a zero value (0.0), from which any value multiplied by them will remain zero, and considered those areas as background. The normal proportional error of 0.15 (15%) was assigned as maximum likelihood (Gemmechis, 2022; Sabree Ali et al., 2020).

For the CA model, the LULC classified image of 2020 was used as the base year, from which files of transition areas and transaction suitable image (probability) produced by MC for 2020 to 2050 were added. The number of cellular automate interaction was considered 30, the same as the number of projected years, and a contiguity filter with a kernel size of 5*5 pixels was used to create spatially explicit contiguous weighing factors so that pixels far from the existing land use class have a lower suitability than those near it (Azizi et al., 2016; Subedi et al, 2013).

Through a multi-objective land allocation process, the weighted suitability maps were created, from which allocations to future land use change and conflicts on allocation are solved by giving a cell weighted as the highest suitable for a particular land use class (Subedi et al, 2013).

To validate the results of the model, a forecast map of 2020 (simulated) was created based on LULC classified maps of 2000 and 2010, which were compared with existing classified maps of 2020 through a Kappa index of agreement (KIA), breached into Kno, Klocation, Klocationstrata and Kstandard (Gemmechis, 2022; Hua, 2017; Al-sharif and Pradhan, 2013). Since all KIA statistics values were above 90%, the model was considered suitable to predict future LULC for 2050 (Subedi et al, 2013).

3.2.9 Ancillary Data

As ancillary data, shapefiles of administrative boundaries, roads and railways, rivers and geology maps were clip and used to delineate the study area, as backgrounds and reference data, to compare and explain the results of image classification (Halder et al., 2021). All data used in this research were aligned with the reference data (study area) and converted into universal transverse mercator projection system, 36 south zone, and datum of world geodetic system 1984 to avoid any error that could come from image distortion (Halder et al., 2021; Bhatta, 2013). This information was obtained from the National Statistical Institute, and processed using GEE (image selection and classification), ArGis 10.2 (mapping and change detection), TerrSet (futures prediction) and Excel (correlation analyse, tabulation and graphic production), all licenced by The University of the Witwatersrand.

3.3 Workflow Process

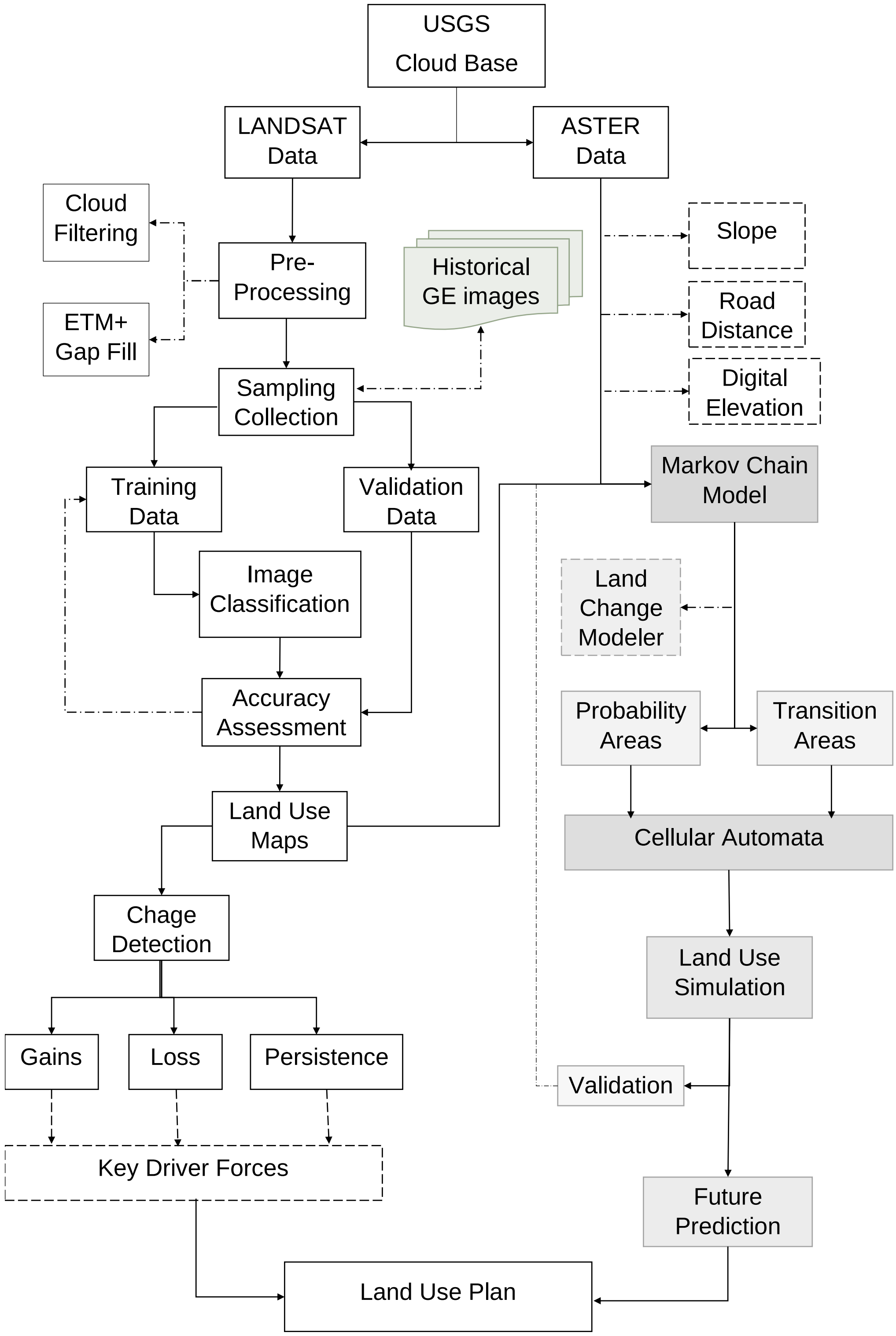

Figure 3. Methodological scheme describing the image classification process and stepwise forecasting with the Cellular Automata-Markov Chain models

CHAPTER FOUR

4. RESULTS

This chapter presents the outputs of this research. The statistics of temporal mapping using the RF algorithm, where the analysis is made within classes in a specific year, showing dominant, increased and decreased classes is outlined. A post-classification analysis to identify the major LULC trends and transitions was performed using ArcGIS 10.2, giving an overview of the dynamic of changes in time. This chapter ends with outputs of the LULC future prediction for the next 30 years, which were forecasted using a CA-MA model in TerrSet software.

4.1 Land Use Land Cover Mapping

To analyse patterns of LULC, five maps of years 1984, 1990, 2000, 2010 and 2020 were prepared using the RF algorithm, through a supervised process. The statistical data (Table 5; Figure 4) summarise the state of the image classification process. For the 1984 reference year, forest was considered the dominant class covering a total area of 319.7 Sq.km, sharing 39.7% of the total area. This class was followed by agriculture, accounting for 218.2 Sq.km (27.1%), baren lands at 99.5 Sq.km (12.4%), wetlands at 81.1 Sq.km (10.1%), rocks with 74.5 Sq.km (9.3%) and waterbodies with 9 Sq.km (1.1%). The smallest area observed was the build-up class with 2.3 Sq.km (0.3%).

In 1990, forests increased (+4%) and continues to be the most significant land class with 355.6 Sq.km (44.2%) of the total area, while agriculture decreased (-5.3%) to 175 Sq.km (21.8%), but remaining the second major class. There was a shift between baren lands and wetlands, with the last being the third most significant class covering a total area of 126.1 Sq.km (15.7%), an increase of (+ 5.6%). This class was followed by rock with 84.1 Sq.km (10.5%), barren 32 Sq.km (4%), build-up 16.6 Sq.km (2.1%) and water bodies with 15 Sq.km (1.9%).

As of 2000, although the forest started to decrease (-8%) it remained the most significant class encompassing 291.2 Sq.km (36.2%) of the total area, followed by agriculture, which slightly increased (+0.2%) to 1771.1 Sq.km (22%). For this year, build-up was the third largest class with a total area of 94 Sq.km (11.7%), changing with wetlands, which was 82.5

Sq.km (10.3%). The smallest classes were barren lands with 74.4 Sq.km (9.2%), rocks with 68 Sq.km (8.5%) and water with 17.2 Sq.km (2.1%).

In 2010, the statistics indicated that forest continued to decrease (-5.3%) but was the most significant class with 248.4 Sq.km, representing 30.9% of the total area. The second class was bare land, which increased (+14%), changing with the agriculture class with a total area of 184.8 Sq.km (23%). Build-up area followed with 123.2 Sq.km (15.3%), rock and wetlands with 81.5 Sq.km (10.1%) and 79.1 Sq.km (9.8%), respectively. At the bottom, agriculture decreased (-13.7%) and waterbodies increased (+0.5%), ending up with a total area of 66.6 Sq.km (8.3%) and 20.8 Sq.km (2.6%), respectively.

The pattern of LULC changed in 2020 with a huge increase (+15.7%) of built-up areas, accounting for 370.78 Sq.km, which was 46.1% of the total area and the most significant class. This class was followed by forest, which decreased (-12.6%) to a total area of 147.20 Sq.km (18.3%), barren lands at 114.91 Sq.km (14.3%), rocks at 101.75 Sq.km (12.7%), wetlands at 48.31 Sq.km (6%), water at 13.08 Sq.km (1.6%), and agriculture decreased (-7.3%) to a total of 8.28 Sq.km (1%).

Table 5. Area covered per square kilometres of the selected land class, for each reference year (1984, 1990, 2000, 2010 and 2020)

Land use land cover class	Area in square kilometres				
	1984	1990	2000	2010	2020
Agriculture	218.2	175.0	177.1	66.6	8.28
Forest	319.7	355.6	291.2	248.4	147.20
Build-up	2.3	16.6	94.0	123.2	370.78
Barren	99.5	32.0	74.4	184.8	114.91
Rock	74.5	84.1	68.0	81.5	101.75
Wetland	81.1	126.1	82.5	79.1	48.31
Waterbody	9.0	15.0	17.2	20.8	13.08
Total	804.3	804.3	804.3	804.3	804.3

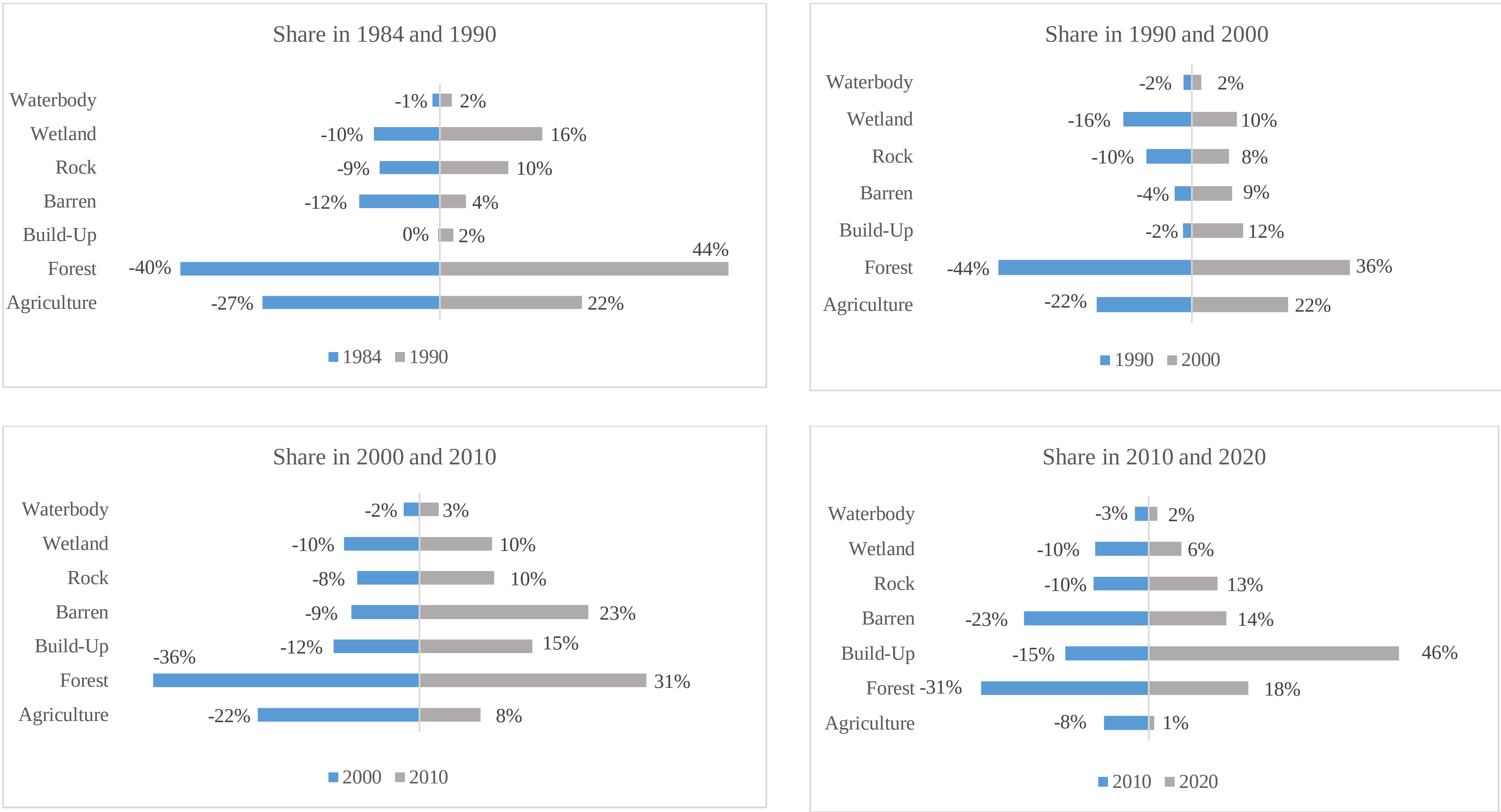

Figure 4. Land use land cover share comparison within each class, between two sequential reference years (1984-1990, 1990-2000, 2000-2010 and 2010-2020)

4.2 Land Use Land Cover Dynamic

The analysis of each class over 36 years (Table 6; Figure 5) shows that although forest was the most significant land cover class with the largest area in almost all reference years (four out of five), it showed a continuously decreasing pattern. A decrease (-21.4%) was observed during the period, with significant changes being observed between 1990 and 2000 (8%) and 2010 and 2020 (12.6%), and a slight increase of 4% observed between 1984 and 1990, accounting to an overall net loss of -172.5 Sq.km, ending with 18.3% of all the area (147.20 Sq.km).

In the same period, agriculture, which was the second most significant class in 1984, decreased by -26.1%, with major changes being observed between 2000 and 2010 (-13.7%) and 2010 and 2020 (7.2%), accounting for a total loss area of -209.9 Sq.km, ending with 1% (8.28 Sq.km) of the total area. In contrast, the build-up class, which was the least significant class in 1984, (0.3%) of the total area, consistently increased between 1984 and 2010 (15.03%) to a total of 120 Sq.km. During the last decade, a huge increase of 30.7% was observed, encompassing 247.55 Sq.km, thus achieving a total of 368.4 Sq.km (45.8%).

The remaining classes showed a floating pattern with increase and decrease events and no significant changes observed between each interval year during the analysis period. In this regard, barren land, which was 12.4% of the total area in 1984, showed a net increase of 10.6% in the following years 1990, 2000 and 2010, which were followed by a decrease of -9% in 2020, ending with 14.3% (114.9 Sq.km) of the total area. Rocks, which was 9.3% in 1984 ended with 12.7% in 2020, with a slightly decline (-2%) observed in 2000.

Wetland, which was 10.1% of the total area in 1984, floated with an improvement of 5.6% in 1990, and declined by 5.4% in 2000. This class remained stable in 2010 with a value of 9.8%, declining (-4%) in 2020, ending with 6% of the total area. Waterbody also floated between 1.1% (1984) to a maximum of 2.6% (2010), showing an increasing and decreasing patterns of less than 1% during the analysis period.

Table 6. Land use land cover area comparison, their share within classes, between two sequential reference years (1984-1990, 1990-2000, 2000-2010 and 2010-2020)

Land use land cover class	Land use land cover area change (Square kilometres)							
	1984 - 1990	Share (%)	1990 - 2000	Share (%)	2000- 2010	Share (%)	2010 - 2020	Share (%)
Agriculture	-43.15	-5.36%	2.08	0.26%	-110.52	-13.74%	-58.30	-7.25%
Forest	35.98	4.47%	-64.48	-8.02%	-42.78	-5.32%	-101.17	-12.58%
Build-up	14.22	1.77%	77.42	9.63%	29.25	3.64%	247.55	30.78%
Barren	-67.52	-8.40%	42.33	5.26%	110.46	13.73%	-69.90	-8.69%
Rock	9.57	1.19%	-16.07	-1.99%	13.44	1.671%	20.30	2.52%
Wetland	44.92	5.59%	-43.56	-5.4%	-3.38	-0.42%	-30.81	-3.83%
Waterbody	6.00	0.75%	2.28	0.28%	3.51	0.437%	- 7.68	-0.95%

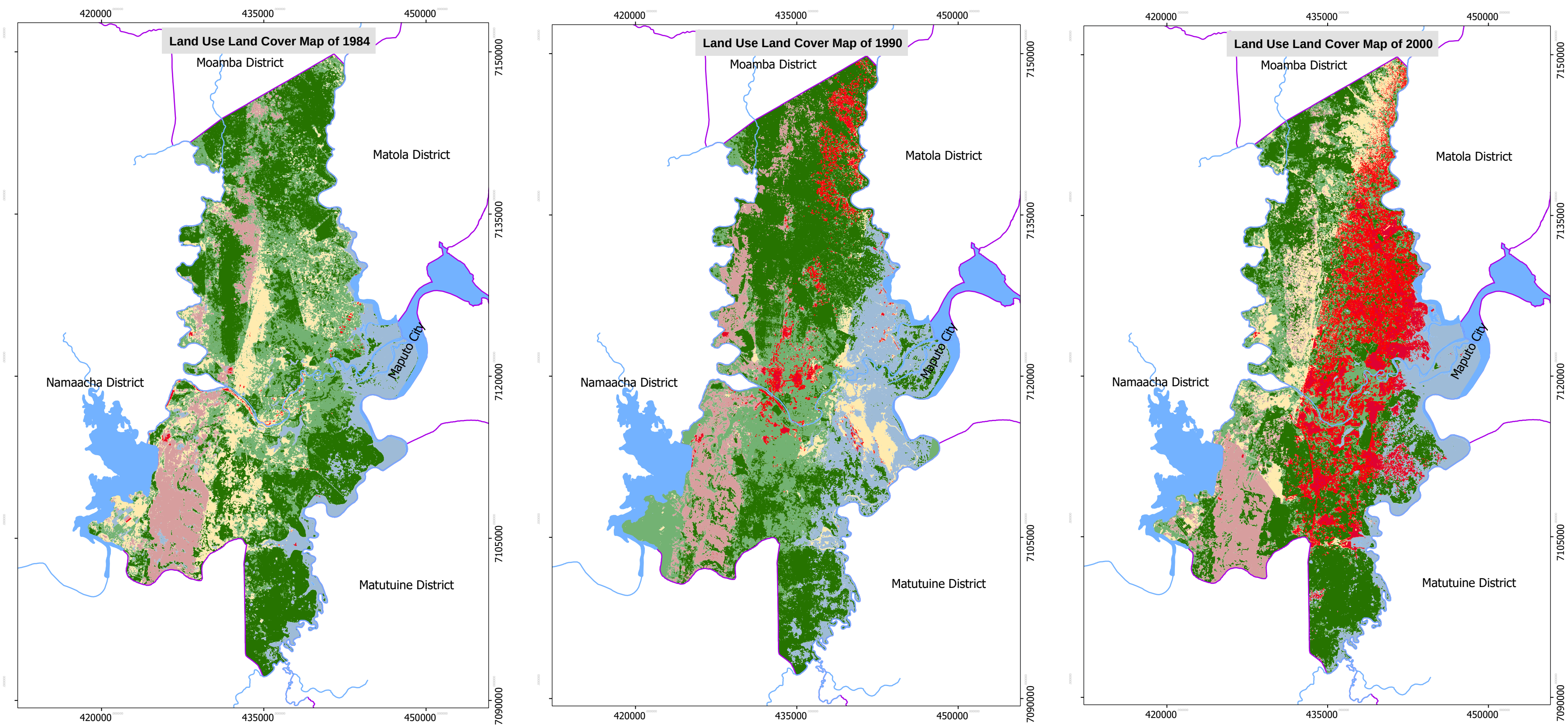
Land Use Land Cover Map of 1984
Moamba District
Matola District
Maputo City
Namaacha District
Matutuine District
420000
435000
450000
7150000
7135000
7120000
7105000
7090000
Land Use Land Cover Map of 1990
Moamba District
Matola District
Maputo City
Namaacha District
Matutuine District
Land Use Land Cover Map of 2000
Moamba District
Matola District
Maputo City
Namaacha District
Matutuine District

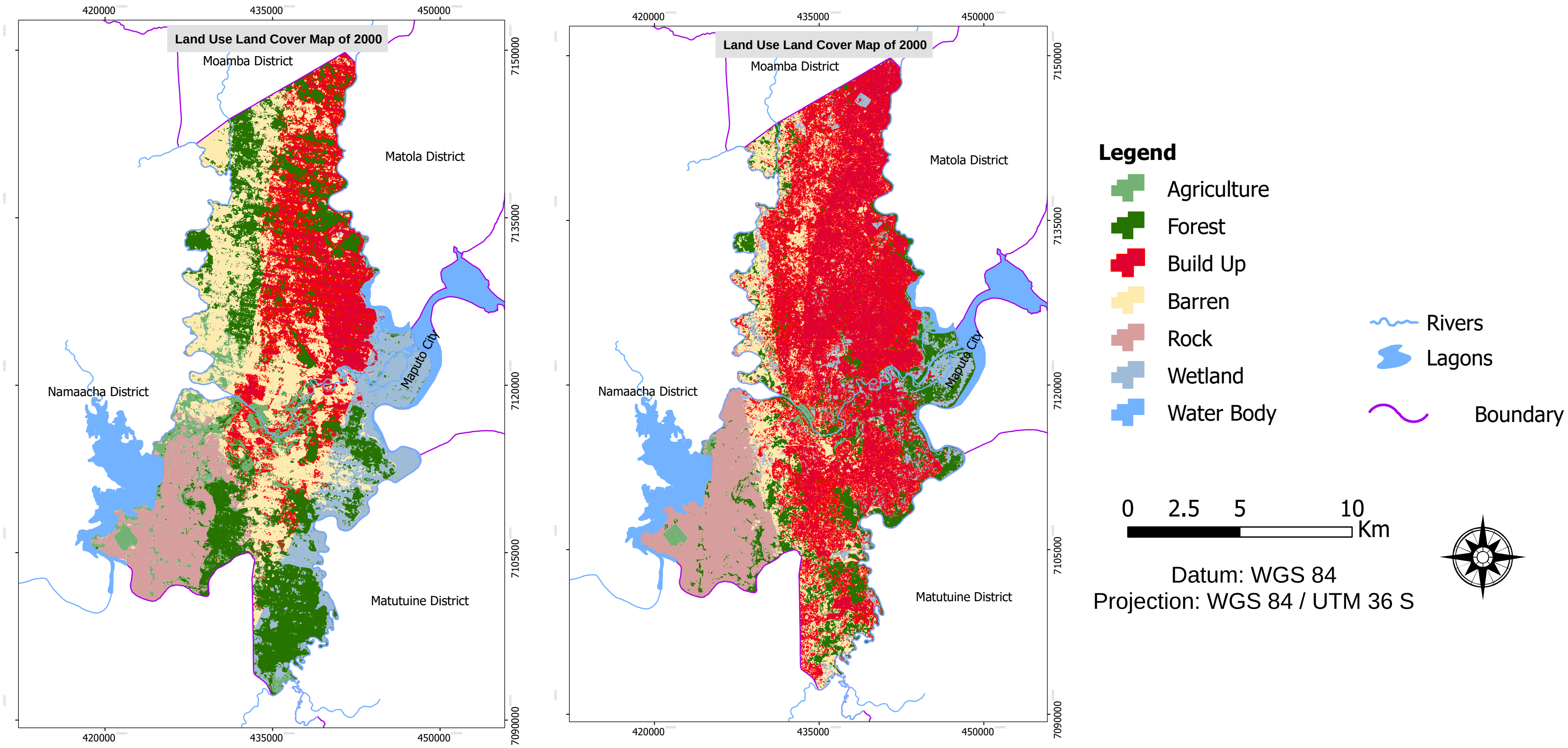

Figure 5. Result of land use land cover analysis using images from Landsat thematic mapper, enhanced thematic mapper plus and operational land imager and thermal infrared sensors, and random forest classifier algorithm, for each reference year (1984, 1990, 2000, 2010 and 2020)

The overall changes between 1984 and 2020 (Table 7; Figure 6) indicated a huge change in the build-up class with a share of 45.8%, followed by rock with 3.4%, barren (1.9%) and waterbody (0.5%). On the other hand, agriculture (-26.1%) decreased the most, followed by forest (-21.4%) and wetlands (-4.1%). The rate of change during the period of analysis was negative per year for agriculture (-5.8%), forest (-4.79%) and wetlands (-0.91%), while positive for build-up areas (10.2%), rock areas (0.76%), barren lands (0.43%) and water bodies (0.11%).

Table 7. Land use land cover area comparison, their percentage and rate of change between 1984 and 2020

Land use land cover (Square kilometre)	Agri-culture	Forest	Build-up	Barren	Rock	Wet-land	Water body
1984	218.2	319.7	2.3	99.5	74.5	81.1	9.0
2020	8.28	147.20	370.78	114.91	101.75	48.31	13.08
Magnitude Change	-209.89	-172.45	368.45	15.37	27.23	-32.83	4.12
% of Change	-0.96	-0.54	158.04	0.15	0.37	-0.40	0.46
Rate of Change	-5.830	-4.790	10.235	0.427	0.757	-0.912	0.114

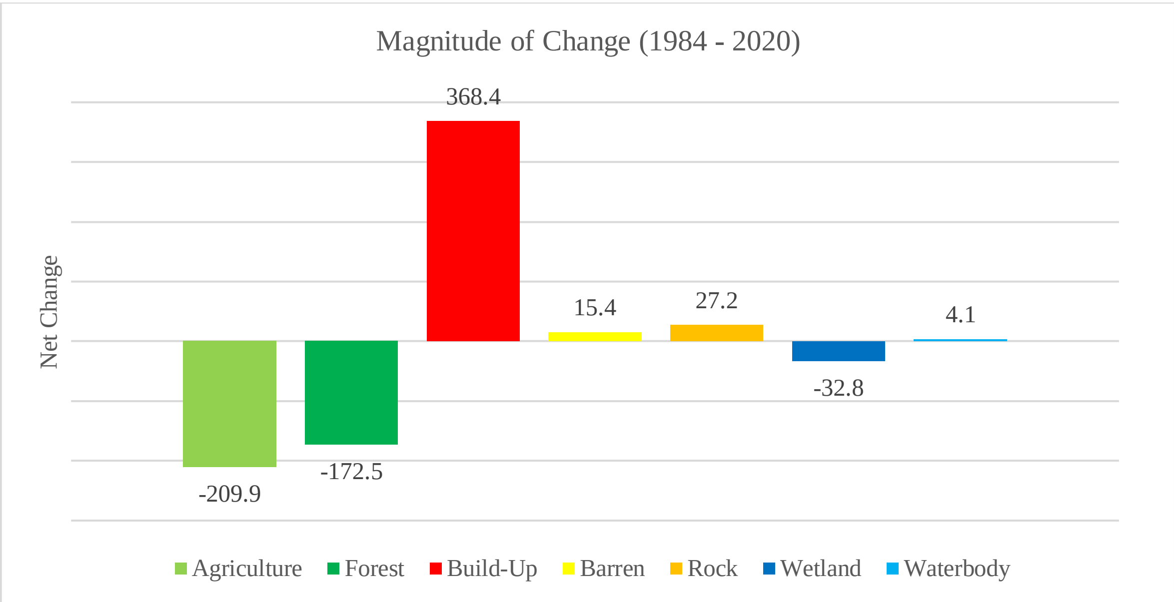

Figure 6. Magnitude of change in square kilometres within each land cover class, between 1984 and 2020

4.3 Accuracy Assessment

According to the results (Table 8 to Table 12), all seven classes i.e., agriculture, forest, build-up, barren, rock, wetlands and waterbody, were assessed and separated from each other above the average 90% threshold accuracy assessment and 0.8799 kappa coefficient (Figure 7), which indicates a very good straightness agreement (Meli Fokeng et al., 2020; Bhatta, 2013). Additionally, other parameters (Table 13) i.e., user accuracy and producer accuracy were taken into account to clarify the classification process.

Analysing each class per year, in 1984, the values of overall accuracy assessment were 87% and a 0.8485 kappa coefficient. The user accuracy ranged from 50% to 100%, with barren being the lowest, followed by agriculture at 73%, build-up at 80% and waterbody at 92%. The highest value was observed in forests, rocks and wetlands. The producer accuracy ranged from 83% to 100%, with the lowest value being barren (71%), followed by wetlands (83%), rocks and forest (86% each), build-up areas (88%), agriculture (92%), and the highest was waterbody (100%).

From the matrix of 1990, the results indicated an overall accuracy of 90% and a kappa coefficient of 0.8877, with the lower user accuracy being 73% for baren, 80% for agriculture, 83% for forest and 92% for build-up. The highest was in rock, wetlands and water with 100%. The lowest producer accuracy was from forest with 83%, build-up with 85%, agriculture and baren with 89% each, and rocks and waterbody with 92% each. The highest was wetland with 100%.

In 2000, the overall accuracy was 89.5% with a kappa coefficient of 0.8746, with the lower user accuracy ranging from 64% for wetlands, 81% for baren, 92% for agriculture, and 95% for build-up. The rock class was the highest with 100%. The lowest producer accuracy was from the forest class with 60%, build-up and waterbodies with 88% each, and baren with 93%. The highest was agriculture, rock and wetlands with 100% each.

For 2010, the overall accuracy was 90.9% with a kappa coefficient of 0.8926, with the lower user accuracy ranging from 86% for baren, 87% for forest and 88% for build-up, while the highest was rock, wetland and waterbody with 100%. On the other hand, the lowest producer accuracy was 80% for baren, 82% for build-up and 87% for forest. The highest was agriculture, rock and wetlands with 100%.

In the last year, 2020, the error matrix indicates an overall accuracy value of 91.2% with a kappa coefficient of 0.8964. The lowest user accuracy was 67% from the wetland, followed by 78% from baren, 86 from build-up and 94% from agriculture, while the highest was forest and rock with 100%. The producer accuracy results were 70% for baren as the lowest, 86% for wetlands, 92% for forest and build-up, 93% for rock and 94% for waterbodies. The highest value was observed in agriculture with 100%.

Table 8. Random Forest classifier overall accuracy and kappa coefficient values mapping land use land cover for 1984

1984										
Land use land cover class	Reference Class							Row Total	Commission Error (%)	User Accuracy (%)
	Agriculture	Forest	Build-up	Barren	Rock	Wetland	Waterbody			
Agriculture	11	3	0	1	0	0	0	15	27	73
Forest	0	19	0	0	0	0	0	19	0	100
Build-up	0	0	7	1	0	0	0	8	13	88
Barren	1	0	1	5	2	1	0	10	50	50
Rock	0	0	0	0	12	0	0	12	0	100
Wetland	0	0	0	0	0	10	0	10	0	100
Waterbody	0	0	0	0	0	1	11	12	8	92
Column Total	12	22	8	7	14	12	11	86		
Omission Error (%)	8	14	13	29	14	17	0			
Producer's Accuracy (%)	92	86	88	71	86	83	100			
Random Accuracy (%)	2	6	1	1	2	2	2	16		
Overall Accuracy (Pa)	87.2%									
Kappa Coefficient (Pr)	0.8485									

Table 9. Random Forest classifier overall accuracy and kappa coefficient values mapping land use land cover for 1990

1990										
Land use land cover class	Reference Class							Row Total	Commission Error (%)	User Accuracy (%)
	Agriculture	Forest	Build-up	Barren	Rock	Wetland	Waterbody			
Agriculture	8	1	0	0	0	0	1	10	20	80
Forest	1	5	0	0	0	0	0	6	17	83
Build-up	0	0	11	1	0	0	0	12	8	92
Barren	0	0	2	8	1	0	0	11	27	73
Rock	0	0	0	0	11	0	0	11	0	100
Wetland	0	0	0	0	0	11	0	11	0	100
Waterbody	0	0	0	0	0		12	12	0	100
Column Total	9	6	13	9	12	11	13	73		
Omission Error (%)	11	17	15	11	8	0	8			
Producer's Accuracy (%)	89	83	85	89	92	100	92			
Random Accuracy (%)	2	1	3	2	2	2	3	15		
Overall Accuracy (Pa)	90.4%									
Kappa Coefficient (Pr)	0.8874									

Table 10. Random Forest classifier overall accuracy and kappa coefficient values mapping land use land cover for 2000

2000										
Land use land cover class	Reference Class							Row Total	Commission Error (%)	User Accuracy (%)
	Agriculture	Forest	Build-up	Barren	Rock	Wetland	Waterbody			
Agriculture	12	0	0	0	0	0	1	13	8	92
Forest	0	6	0	0	0	0	0	6	0	100
Build-up	0	0	21	1	0	0	0	22	5	95
Barren	0	0	3	13	0	0	0	16	19	81
Rock	0	0	0	0	11	0	0	11	0	100
Wetland	0	4	0	0	0	7	0	11	36	64
Waterbody	0	0	0	0	0	0	7	7	0	100
Column Total	12	10	24	14	11	7	8	86		
Omission Error (%)	0	40	13	7	0	0	13			
Producer's Accuracy (%)	100	60	88	93	100	100	88			
Random Accuracy (%)	2	1	7	3	2	1	1	17		
Overall Accuracy (Pa)	89.5%									
Kappa Coefficient (Pr)	0.8746									

Table 11. Random Forest classifier overall accuracy and kappa coefficient values mapping land use land cover for 2010

2010										
Land use land cover class	Reference Class							Row Total	Commission Error (%)	User Accuracy (%)
	Agriculture	Forest	Build-up	Barren	Rock	Wetland	Waterbody			
Agriculture	11	1	0	1	0	0	0	13	15	85
Forest	0	13	1	1	0	0	0	15	13	87
Build-up	0	1	14	1	0	0	0	16	13	88
Barren	0	0	2	12	0	0	0	14	14	86
Rock	0	0	0	0	5	0	0	5	0	100
Wetland	0	0	0	0	0	11	0	11	0	100
Waterbody	0	0	0	0	0	0	14	14	0	100
Column Total	11	15	17	15	5	11	14	88		
Omission Error (%)	0	13	18	20	0	0	0			
Producer's Accuracy (%)	100	87	82	80	100	100	100			
Random Accuracy (%)	2	3	4	3	0	2	3	15		
Overall Accuracy (Pa)	90.9%									
Kappa Coefficient (Pr)	0.8926									

Table 12. Random Forest classifier overall accuracy and kappa coefficient values mapping land use land cover for 2020

2020										
Land use land cover class	Reference Class							Row Total	Commission Error (%)	User Accuracy (%)
	Agriculture	Forest	Build-up	Barren	Rock	Wetland	Waterbody			
Agriculture	16	0	0	0	0	0	1	17	6	94
Forest	0	12	0	0	0	0	0	12	0	100
Build-up	0	1	12	1	0	0	0	14	14	86
Barren	0	0	0	7	1	1	0	9	22	78
Rock	0	0	0	0	13	0	0	13	0	100
Wetland	0	0	1	2	0	6	0	9	33	67
Waterbody	0	0	0	0	0	0	17	17	0	100
Column Total	16	13	13	10	14	7	18	91		
Omission Error (%)	0	8	8	30	7	14	6			
Producer's Accuracy (%)	100	92	92	70	93	86	94			
Random Accuracy (%)	3	2	2	1	2	1	4	15		
Overall Accuracy (Pa)	91.2%									
Kappa Coefficient (Pr)	0.8964									

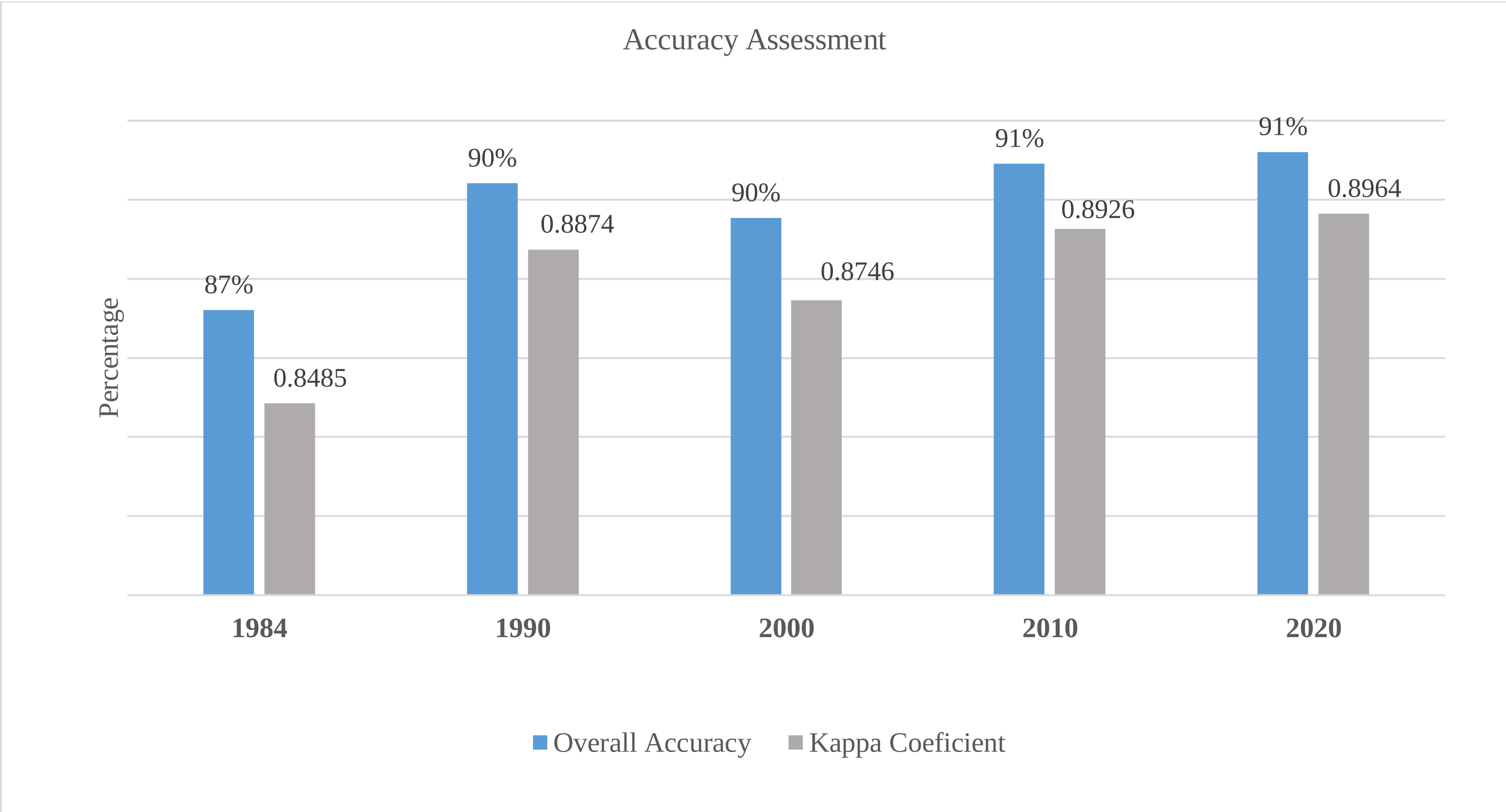

Figure 7. Random forest classifier overall accuracy and kappa coefficient values mapping land use land cover classes at ten-year intervals, 1984, 1990, 2000, 2010 and 2020

Table 13. Accuracy assessment result derived from random forest classification of Landsat image from sensor TM, ETM+, and OLI/TIR, between 1984 and 2020

Land use land cover class	1984		1990		2000		2010		2020	
	User Accuracy (%)	Producer Accuracy (%)	User Accuracy (%)	Producer Accuracy (%)	User Accuracy (%)	Producer Accuracy (%)	User Accuracy (%)	Producer Accuracy (%)	User Accuracy (%)	Producer Accuracy (%)
Agriculture	73%	92%	80%	89%	92%	100%	85%	100%	94%	100%
Forest	100%	86%	83%	83%	100%	60%	87%	87%	100%	92%
BuildUp	88%	88%	92%	85%	95%	88%	88%	82%	86%	92%
Barren	50%	71%	73%	89%	81%	93%	86%	80%	78%	70%
Rock	100%	86%	100%	92%	100%	100%	100%	100%	100%	93%
Wetland	100%	83%	100%	100%	64%	100%	100%	100%	67%	86%
Waterbody	92%	100%	100%	92%	100%	88%	100%	100%	100%	94%

4.4 Change Detention and Land Transformation

To assess the direction of changes in LULC, four cross-tabulation (from – to) matrices were produced through a pixel-by-pixel comparison process of two classified images taken in different periods, which provided detailed quantitative and qualitative information of changes between classes (Goswami et al., 2022; Gudo et al., 2022; Bagarinao et al., 2020; Dessu et al., 2020; Lu et al., 2004). Therefore, the change detection analysis was performed in two steps, short-term and long-term change analysis.

Short-term analyse change analysis was performed analysis comparing periods of ten years, between 1980 and 1990, 1990 and 2000, 2000 and 2010, and 2010 and 2020 (Table 14 to17; Figure 8; Table B1 to B4). According to Bell et al. (2020) and Woodcock et al. (2020), short-time frame provides more inputs to environmental issues giving simple explanations for any specific LULC transition at a different magnitude, making data more comparable, and avoiding errors from datasets, such as low image quality and satellite gap errors.

Long-term change analysis was used comparing the period of 40 years, between 1980 and 2020 (Table 18; and Figure 9 to 10; Table B5), showing the gains, losses and persistence to change, along with LULC's change direction. Long-time frame provides valuable evidence to detect and characterise trends in historical data, as it can uncover the persistent events that occurred gradually due to political, institutional, or economic conditions, as well as natural events and matters of human settlement. It minimises omission errors (Woodcock et al. 2020, and Lunetta et al. 2004).

4.4.1 **Short-Term Change Analyse**

The from – to matrix of 1984 to 1990 result, agriculture, forest and barren was the most notable class with the highest changing area. Agriculture was the class with largest decreasing area, losing a total of 148 Sq.km by conversion to forest in 78.4 Sq.km, wetlands 34 Sq.km, barren 11.3 Sq.km and only 3.3 Sq.km for build-up class. From its total area (218 Sq.km), almost 70 Sq.km remained unchanged. Agriculture showed a high value of swapping area (253.24 Sq.km).

Forest (the dominant class) remained unchanged (212.8 Sq.km out of a total 319.5 Sq.km), which was the highest persistence rate, while 106.7 Sq.km was lost. From the total lost area, 39.5 Sq.km were converted to agriculture, 37 Sq.km to wetlands, 11.1 Sq.km to baren lands, 6.7 Sq.km to build-up areas and 0.9 Sq.km to waterbody. The swapping area of forest was the second highest (249.28 Sq.km).

Barren class, which lost 94.6 Sq.km out of 99.5 Sq.km, was the third major loss class; 46.3 Sq.km was converted to agriculture, 24 Sq.km to forest, 11.3 Sq.km to rock class and 5.3 Sq.km to wetlands. The unchanged area was 4.9 Sq.km, and the swapping area was 121.81 Sq.km.

For the period of 1990 to 2000, forest lost the highest area, 186.5 Sq.km out of 355.4 Sq.km, which was converted to agriculture at 75.7 Sq.km, barren lands at 37.8 Sq.km, build-up at 31.4 Sq.km, wetlands at 21.4 Sq.km, and waterbody at 0.4 Sq.km, as the lowest lost area. A total of 168 Sq.km remain unchanged and 308.64 Sq.km swapped.

Agriculture, the second class with the largest loss, 112.3 Sq.km out of 174.9 Sq.km was converted to forest at 57.4 Sq.km, build-up at 20.5 Sq.km, barren at16.4 Sq.km, and, the lowest, wetland and waterbody at 2.6 Sq.km and 1.4 Sq.km, respectively. From the total, 62.6 Sq.km remained unchanged while 226.6 Sq.km swapped to other classes. The rock class, which lost 50.6 Sq.km out of 84 Sq.km, was converted to forest (18.4 Sq.km), agriculture (17.7 Sq.km), and barren land (13.6 Sq.km). A total of 33.4 Sq.km remained unchanged, while 85.25 Sq.km was swapped.

The statistics for the period of 2000 to 2010 indicates that agriculture was a class that lost a major area, with 151.1 Sq.km out of 177 Sq.km. Of this, 55.9 Sq.km was converted to barren lands, 45.4 Sq.km to forest, 36.8 Sq.km to build-up areas, and 25.9 remain unchanged. A total of 191.9 Sq.km was swapped.

Forest was the second class with the largest lost, 144.94 out of 291 Sq.km, which was converted for barren land at 56.5 Sq.km, build-up at 27.8 Sq.km, agriculture at 22.4 Sq.km and wetlands at 17.3 Sq.km, totalling 145.6 Sq.km lost out of 291 Sq.km. A total of 146.1 Sq.km remained unchanged. It also presented the highest value of swapped area, 247.11 Sq.km. The build-up class, which lost 53.9 Sq.km out of 94 Sq.km, was converted mostly to barren land (31.3 Sq.km) and forest (12.9 Sq.km), while 40.1 Sq.km remained unchanged.

The matrix of 2010 to 2020 indicates forest as the class with the major loss, 168.3 Sq.km out of 248.2 Sq.km, which was mostly converted to build-up areas at 109.9 Sq.km, and to barren lands at 38.7 Sq.km. A total of 79.9 Sq.km remained unchanged while 235.46 Sq.km swapped to other classes.

Barren land was the second class with major lost area, 139.4 Sq.km out of 184.7 Sq.km, mostly converted to build-up (115.5 Sq.km), forest (10.9 Sq.km), wetland (9.9 Sq.km) and rock (2.9 Sq.km), and a total of 45.3 Sq.km remained unchanged. The swapped area was 209 Sq.km. The agriculture class continued to decreased with a total loss of 61.2 Sq.km out of 66.5 Sq.km, which was converted to build-up (15.5 Sq.km), forest (14.6 Sq.km) and barren land (12.5 Sq.km). A total of 5.4Sq.km remained unchanged.

Table 14. Detailed outputs of short-term change detection analyse comparing ten years, showing values of persistence, gains and loss, swapping areas, changes and shares, between 1984 and 1990

Land use land cover class	Total 1984	Total 1990	Persistence (P)	Gain (G)	Loss (L)	Swap (S)	Total Change	Absolute Net Change	Share of 1984	Share of 1990
Agriculture	218.2	175.0	69.9	105.04	148.20	253.30	253.24	-0.05	0.27	0.22
Forest	319.7	355.6	212.8	142.60	106.67	249.23	249.28	0.04	0.40	0.44
Build-up	2.3	16.6	0.8	15.78	1.55	17.31	17.33	0.02	0.00	0.02
Barren	99.5	32.0	4.9	27.12	94.60	121.81	121.73	-0.08	0.12	0.04
Rock	74.5	84.1	41.2	42.88	33.33	76.20	76.21	0.01	0.09	0.10
Wetland	81.1	126.1	48.7	77.27	32.31	109.52	109.58	0.06	0.10	0.16
Waterbody	9.0	15.0	6.7	8.22	2.24	10.46	10.46	0.01	0.01	0.02

Table 15. Detailed outputs of short-term change detection analyse comparing ten years, showing values of persistence, gains and loss, swapping areas, changes and shares, between 1990 and 2000

Land use land cover class	Total 1990	Total 2000	Persistence (P)	Gain (G)	Loss (L)	Swap (S)	Total Change	Absolute Net Change	Share of 1990	Share of 2000
Agriculture	175.0	177.1	62.63	114.36	112.28	226.63	226.63	0.00	0.22	0.22
Forest	355.6	291.2	168.92	122.08	186.49	308.64	308.56	-0.08	0.44	0.36
Build-up	16.6	94.0	5.31	88.66	11.24	99.80	99.90	0.10	0.02	0.12
Barren	32.0	74.4	0.79	73.53	31.24	104.72	104.77	0.05	0.04	0.09
Rock	84.1	68.0	33.40	34.58	50.65	85.25	85.23	-0.02	0.10	0.08
Wetland	126.1	82.5	51.10	31.27	74.87	106.19	106.14	-0.05	0.16	0.10
Waterbody	15.0	17.2	14.01	3.21	0.93	4.14	4.15	0.00	0.02	0.02

Table 16. Detailed outputs of short-term change detection analyse comparing ten years, showing values of persistence, gains and loss, swapping areas, changes and shares, between 2000 and 2010

Land use land cover class	Total 2000	Total 2010	Persistence (P)	Gain (G)	Loss (L)	Swap (S)	Total Change	Absolute Net Change	Share of 2000	Share of 2010
Agriculture	177.1	66.6	25.87	40.65	151.11	191.90	191.76	-0.14	0.22	0.08
Forest	291.2	248.4	146.06	102.16	144.95	247.16	247.11	-0.05	0.36	0.31
Build-up	94.0	123.2	40.10	83.11	53.87	136.94	136.98	0.04	0.12	0.15
Barren	74.4	184.8	29.30	155.43	45.02	200.30	200.44	0.14	0.09	0.23
Rock	68.0	81.5	44.51	36.93	23.48	60.40	60.41	0.02	0.08	0.10
Wetland	82.5	79.1	53.17	25.88	29.21	55.08	55.08	0.00	0.10	0.10
Waterbody	17.2	20.8	15.09	5.62	2.12	7.74	7.74	0.00	0.02	0.03

Table 17. Detailed outputs of short-term change detection analyse comparing ten years , showing values of persistence, gains and loss, swapping areas, changes and shares, between 2010 and 2020

Land use land cover class	Total		Persistence (P)	Gain (G)	Loss (L)	Swap (S)	Total Change	Absolute Net Change	Share of 2010	Share of 2020
	2010	2020								
Agriculture	66.6	8.28	5.37	2.91	61.15	64.13	64.06	-0.07	0.08	0.01
Forest	248.4	147.20	79.93	67.05	168.29	235.46	235.34	-0.13	0.31	0.18
Build-up	123.2	370.78	104.01	266.70	19.19	285.58	285.89	0.31	0.15	0.46
Barren	184.8	114.91	45.29	69.54	139.44	209.07	208.98	-0.09	0.23	0.14
Rock	81.5	101.75	70.26	31.44	11.18	42.59	42.61	0.03	0.10	0.13
Wetland	79.1	48.31	19.26	29.02	59.75	88.81	88.78	-0.04	0.10	0.06
Waterbody	20.8	13.08	11.31	1.74	9.38	11.13	11.12	-0.01	0.03	0.02

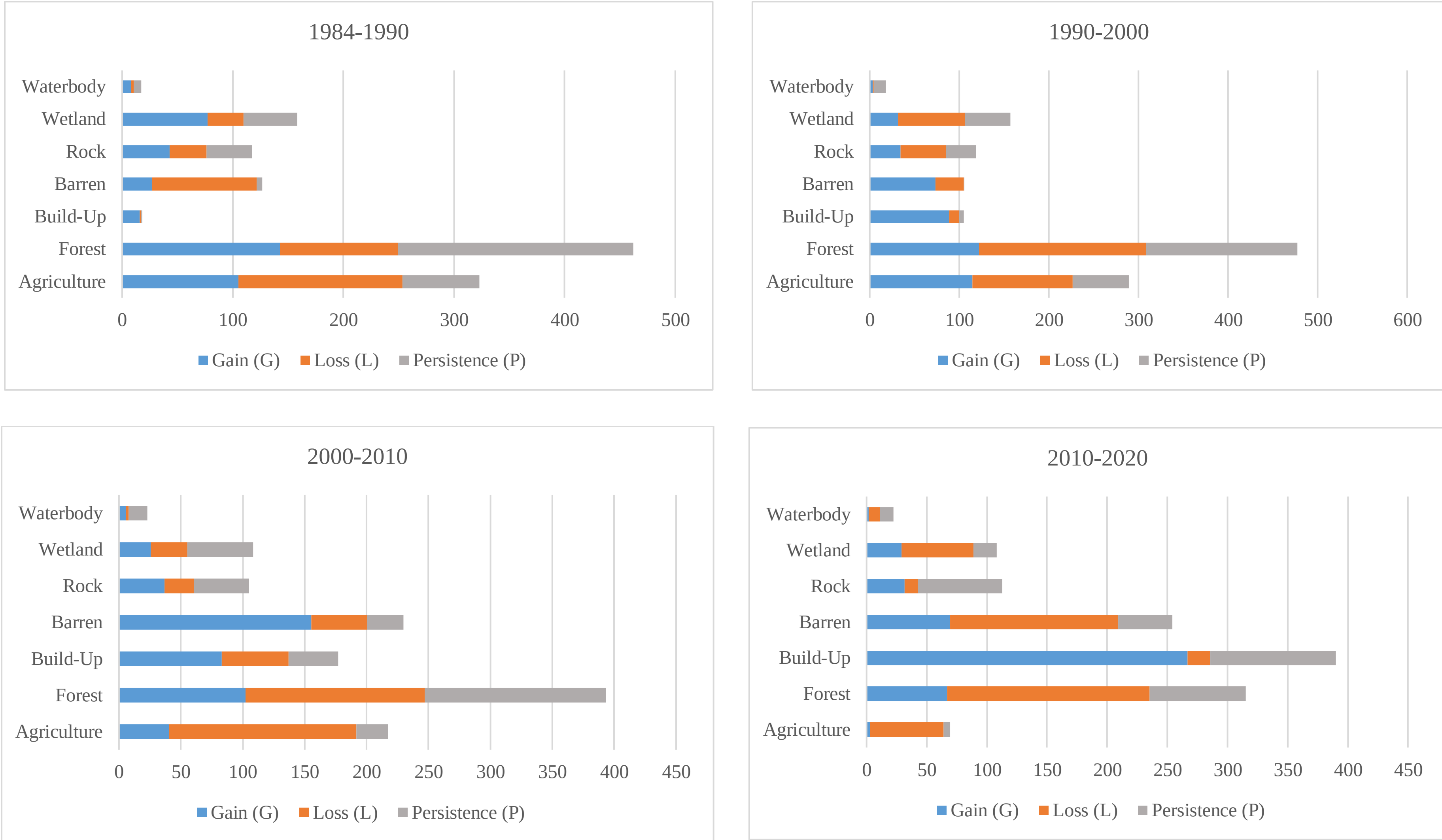

Figure 8. Land use land cover quantitative information (gains, loss and persistence) within each class and between two sequential reference year (1984-1990, 1990-2000, 2000-2010, and 2010-2020)

4.4.2 Long Term Change Analyse

Analysing statistics over a period of 36 years indicates that great areas of forest, agriculture, baren and wetlands were lost by converting into build-up areas. A total of 246.8 Sq.km out of 319.5 Sq.km of forest area were lost by converting to another class. Specifically, 170.3 Sq.km of forest areas were converted to build-up class, 49 Sq.km to barren land, 13.6 Sq.km to wetlands, and almost 73 Sq.km remained unchanged. During this period, forest class had a net gain area of 74 Sq.km.

Agriculture, which was the class with the second largest loss, 216.1 Sq.km out of 218.1 Sq.km, was converted to build-up (127 Sq.km), barren land (33.4 Sq.km), forest (24.8 Sq.km) and wetlands (11.4 Sq.km) as the major changes. Baren land also changed, with 83.8 Sq.km out of 99.5 Sq.km lost, by converting into build-up areas (47.9 Sq.km), rock areas (20.6 Sq.km), forest (9.5 Sq.km) and wetlands (3.4 Sq.km). Only 2 Sq.km of this class remained unchanged, while 222.6 Sq.km was swapped to other classes. Other classes showed values that were not significant but important for change analysis.

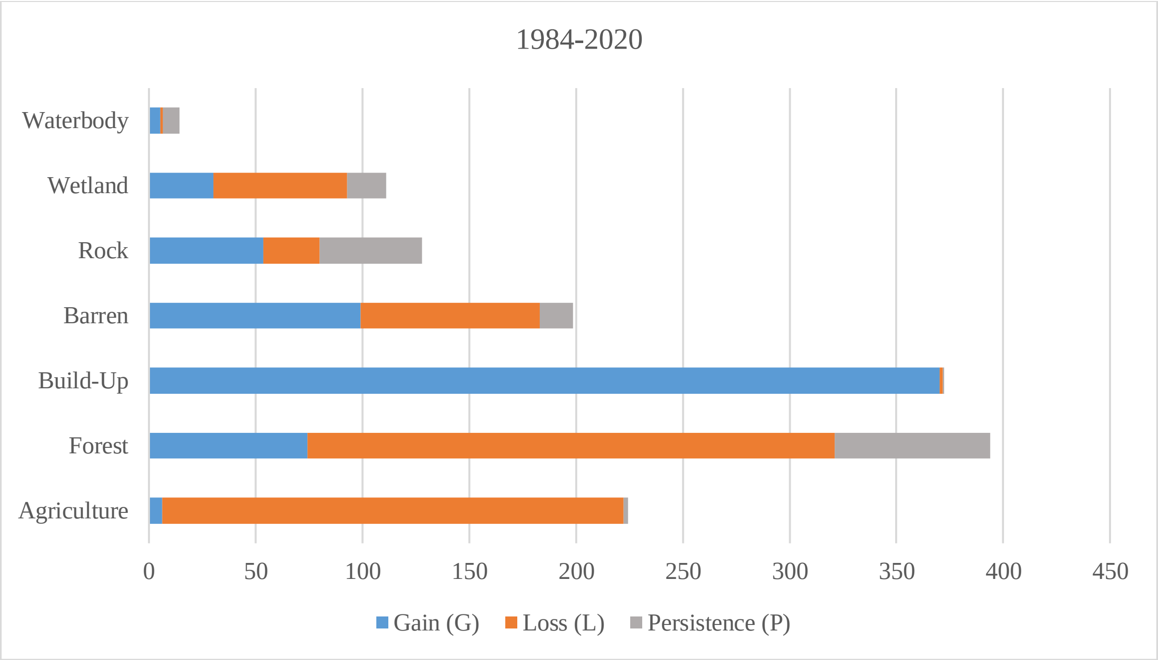

Figure 9. Land use land cover quantitative information (gains, loss and persistence) within each class and between two reference years (1984 and 2020)

Table 18. Detailed outputs of long-term change detection analyse comparing 36 years, showing values of persistence, gains and loss, swapping areas, changes and shares, between 1984 and 2020

Land use land cover class	Total 1984	Total 2020	Persistence (P)	Gain (G)	Loss (L)	Swap (S)	Total Change	Absolute Net Change	Share of 1984	Share of 2020
Agriculture	218.17	8.28	2	6.26	216.05	222.57	222.31	-0.26	0.27	0.01
Forest	319.65	147.20	72.7	74.32	246.81	321.34	321.13	-0.21	0.40	0.18
Build-up	2.33	370.78	0.6	370.13	1.76	371.43	371.89	0.46	0.00	0.46
Barren	99.55	114.91	15.7	99.15	83.82	182.94	182.96	0.02	0.12	0.14
Rock	74.51	101.75	48.1	53.53	26.36	79.85	79.89	0.03	0.09	0.13
Wetland	81.14	48.31	18.2	30.09	62.80	92.93	92.89	-0.04	0.10	0.06
Waterbody	8.96	13.08	7.8	5.27	1.16	6.43	6.43	0.01	0.01	0.02

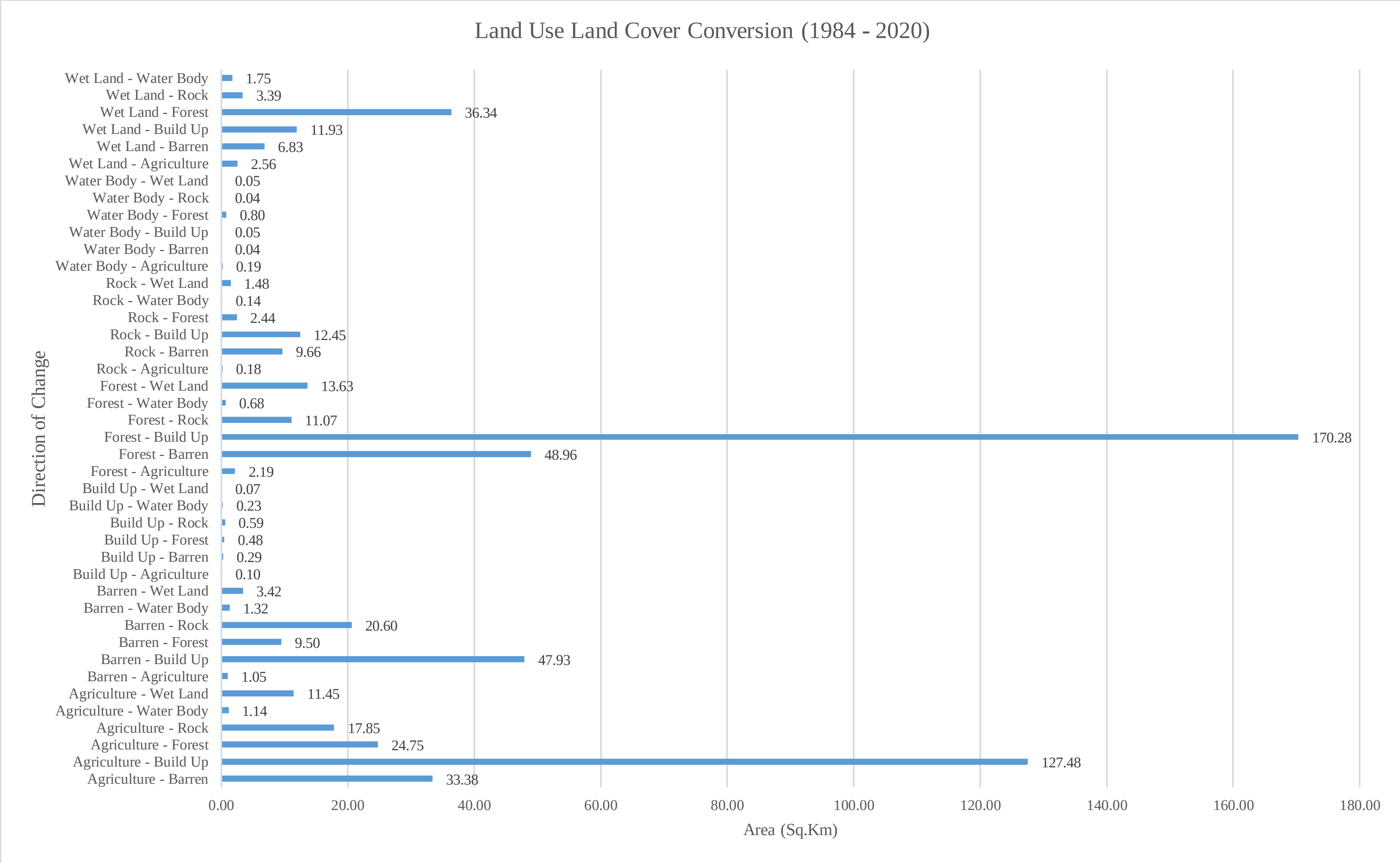

Figure 10. Direction of change within each class of land use land cover, during the study period (1984 and 2020)

4.5 Population Growth and Land Transformation

From the results of Pearson's analysis test (Table 19), build-up and rock classes have a strong and positive correlation with population growth, with (r) values of 0.997 and 0.773, respectively, indicating that an increase in the population variable will increase the other variables (LULC). On the other hand, forests with an (r) value of (-0.974), agriculture (r= -0.923), and wetlands (r = -0.786) indicate a strong but negative correlation. Thus, indicating that the increase in one variable will decreases the other. A weak correlation was observed in barren land and waterbodies, with r = 0.402 and r = 0.173, respectively, which means that none of the variables can account for the change into another.

Investigating the relationship between LULC uncovers that forest and agriculture have a strong negative correlation with the build-up (-0.968 and -0.901) and rock classes (-0.711 and -0.805), respectively, while the forest class was strongly positively correlated only with wetlands (0.890), and agriculture was strongly positively correlated with forest (0.907). The build-up class was strongly correlated with rocks (0.792) and negatively correlated with wetlands (-0.786). Moderately correlated, agriculture had a positive (0.639) correlation with wetlands and a negative (-0.581) correlation with barren, while forests had a negative (-0.557) correlation with barren lands. The remaining were either positive or negative weak correlations, therefore not considerable.

Observing the results of the linear regression model (Figure 11), build-up, forest and agriculture presented a strong linear relationship, with a coefficient of determination (R2) values of 0.967, 0.9528 and 0.8944, respectively. Although, as build-up was positively correlated, these results reveal that for every 1% increase of in the population, build-up will increase by 0.96 Sq.km, while for forest and agriculture, which were negatively correlated, will decrease by 0.95 and 0.89 Sq.km, respectively.

For the rock and wetlands classes, for which the relationship was moderate with R2 values of 0.7088 and 0.6142, for every 1% increase in the population, it will the rock class will increase by 0.70 Sq.km and wetland will decrease by 0.61 Sq.km. Barren lands and waterbody, with R2 values of 0.2147 and 0.0071, presented a weak or insignificant relationship with population.

Table 19. Output of the correlation analyse (Pearson test) between population growth and land cover classes, over 40 years (1980-2020)

	Population	Agriculture	Forest	BuildUp	Barren	Rock	Wetland	Waterbody
Population	1.000							
Agriculture	-0.923	1.000						
Forest	-0.975	0.907	1.000					
BuildUp	0.997	-0.901	-0.968	1.000				
Barren	0.403	-0.581	-0.557	0.352	1.000			
Rock	0.774	-0.805	-0.711	0.792	0.164	1.000		
Wetland	-0.787	0.639	0.890	-0.786	-0.602	-0.406	1.000	
Waterbody	0.143	-0.360	-0.102	0.074	0.409	-0.121	0.107	1.000

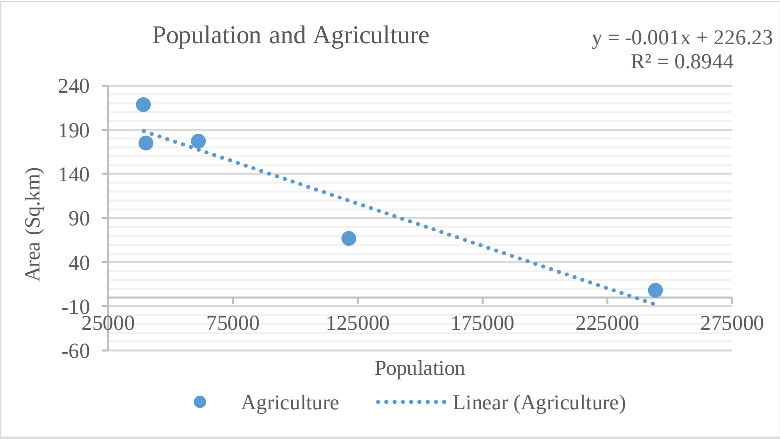

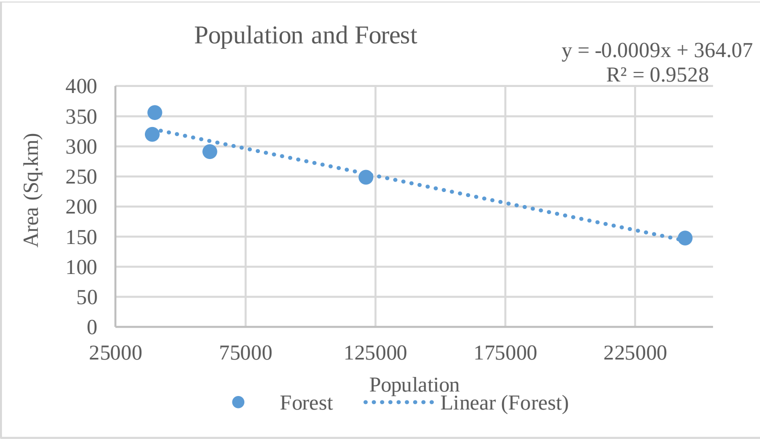

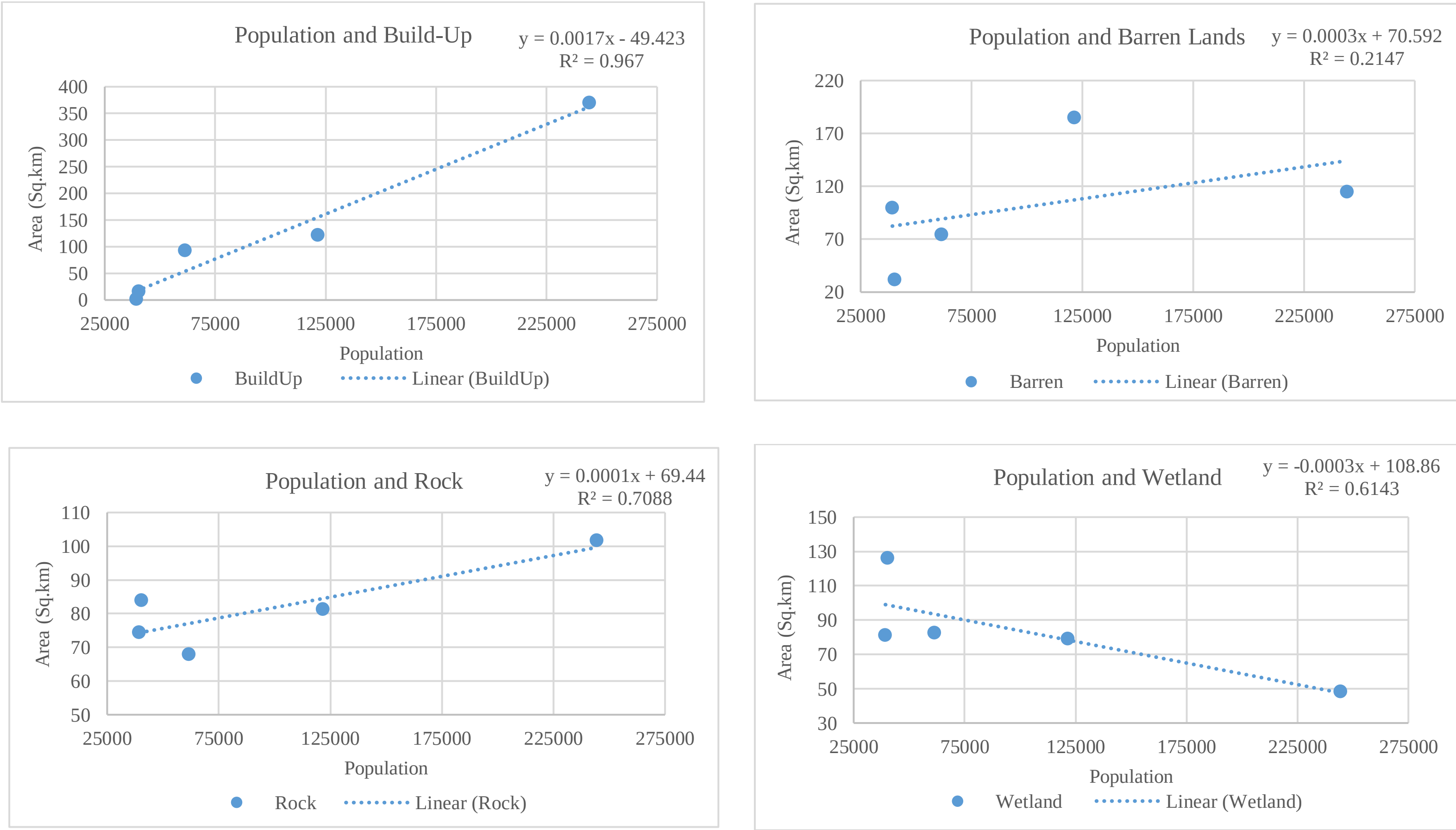

Figure 11. Relationship analyses between population growth and land use land cover classes, over 40 years (1980-2020)

4.6 Land Use Land Cover Future Predicting

4.6.1 Transition Probability Matrix

From the transition matrix (Table 21) generated by the CA-MC models, all classes are expected to change to build-up areas, which is seen as the major influential force due to a rapidly growing population. The matrix derived that build-up and rock are classes with the highest probability of remaining the same class by 2050, with stability values of 63% and 54%, respectively.

Other classes have a very low probability, with agriculture (0.31%) losing 99% of its area, of which 54% is expected to be transformed into build-up areas, and 10% into forest. Wetlands (5.04%) will lose 94% of its area to build-up (64%), forest (15%) and barren lands (10%). Barren land (7.7% of probability) will lose 92% to build-up areas (73%) and forest (10%), while forest class will lose 90% of its area mainly to build-up and barren lands with 69% and 10%, respectively.

Table 20. Matrix of transition probability area, calculated using land use maps of 2020 and forecasted for 2050

	2050								
2020	Agri-culture	Forest	Build-up	Barren	Rock	Wet-lands	Water body	Total	Loss
Agriculture	0.0031	0.1064	0.5395	0.0985	0.2048	0.0451	0.0026	1	0.9969
Forest	0.0031	0.0987	0.6944	0.1001	0.0495	0.0516	0.0026	1	0.9013
Build-up	0.0046	0.1453	0.6376	0.1214	0.0135	0.0736	0.0041	1	0.3625
Barren	0.0032	0.1037	0.7369	0.077	0.0238	0.0527	0.0028	1	0.9231
Rock	0.0034	0.0735	0.2474	0.099	0.5451	0.0306	0.0011	1	0.4550
Wetlands	0.0046	0.1515	0.6431	0.1063	0.0335	0.0504	0.0105	1	0.9495
Waterbody	0.0262	0.1537	0.2394	0.0778	0.3357	0.0277	0.1395	1	0.8605
Total	0.0482	0.8328	3.7383	0.6801	1.2059	0.3317	0.1632	7	5.4488
Gain	0.0451	0.7341	3.1007	0.6031	0.6608	0.2813	0.0237		

4.6.2 Cellular Automata-Markov Model Validation

Using a validation module on TerrSet software, the simulated map of 2050 was compared to a reference map of 2020, downloaded from Google Earth. The results were derivate for the KIA statistic for quantity and location (Table 22), which are differentiated between error and agreement (Merhej et al., 2022).

The result indicates a Kno value of 0.9004, Klocation of 0.9004, Klocationstrata of 0.8059 and Kstandard of 0.8607. From these results, CA-MC can be considered a valid model as it has the ability to predict future LULC by allocating grid cell location to its near perfect, as all K-statistics are greater than 0.80, compared to one, which is a perfect agreement (Subedi et al, 2013).

Table 21. Statistic of kappa index of agreement, derived from the Cellular Automata-Markov model, by comparison of the classified image of 2020 and forecasted for 2050

Agreement				Kappa Indices	
AgreeGridCell	0.5059	DisaAgreeGridCell	0.0560	Kstandard	0.8607
AgreeQuantity	0.2472	DisaAgreeQuantity	0.0659	Kno	0.9004
AgreeChance	0.1250			Klocation	0.9004
				Klocation Strata	0.8059

4.6.3 Predicting Land Use Land Cover for 2050

The simulated map indicates that build-up areas will be the significant class by 2050 (Table 23; Figure 12; Table B6) if the management conditions remain the same as in 2020, with a huge increasing trend of 487.10 Sq.km, accounting for a share of 60.6% of the total area. This value represents a net change of 116.32 Sq.km (14.5%) compared to other classes.

On the other hand, the remaining classes i.e., forest, barren, rock, wetlands, waterbody and agriculture will reduce their total area to 97.79 Sq.km (12.2%), 85.63 Sq.km (10.6%), 78.34 Sq.km (9.74%), 46.99 Sq.km (5.8%), 5.47 Sq.km (0.7%) and 3.2 Sq.km (0.4%), respectively.

The net change between 2020 and 2050 will be reduced 49.41 Sq.km (-6.1%) for forest, 29.56 Sq.km (-3.7%) for barren lands, 23.41 Sq.km (-2.9%) for rock, 7.61 Sq.km (-0.9%) for waterbody, 5.01 Sq.km (-0.6%) for agriculture, and 1.32 (-0.2%) for wetlands.

Table 22. Land use land cover area comparison, their percentage and rate of change, between the classified map of 2020 and forecast for 2050

Land use land cover (Square kilometre)	Agri-culture	Forest	Build-up	Barren	Rock	Wet land	Water body
2000	8.28	147.20	370.78	114.91	101.75	48.31	13.08
2050	3.27	97.79	487.10	85.36	78.34	46.99	5.47
Net Change	-5.01	-49.41	116.32	-29.56	-23.41	-1.32	-7.61
% of Change	-0.60	-0.34	0.31	-0.26	-0.23	-0.03	-0.58
Rate of change	-0.167	-1.647	3.877	-0.985	-0.780	-0.044	-0.254

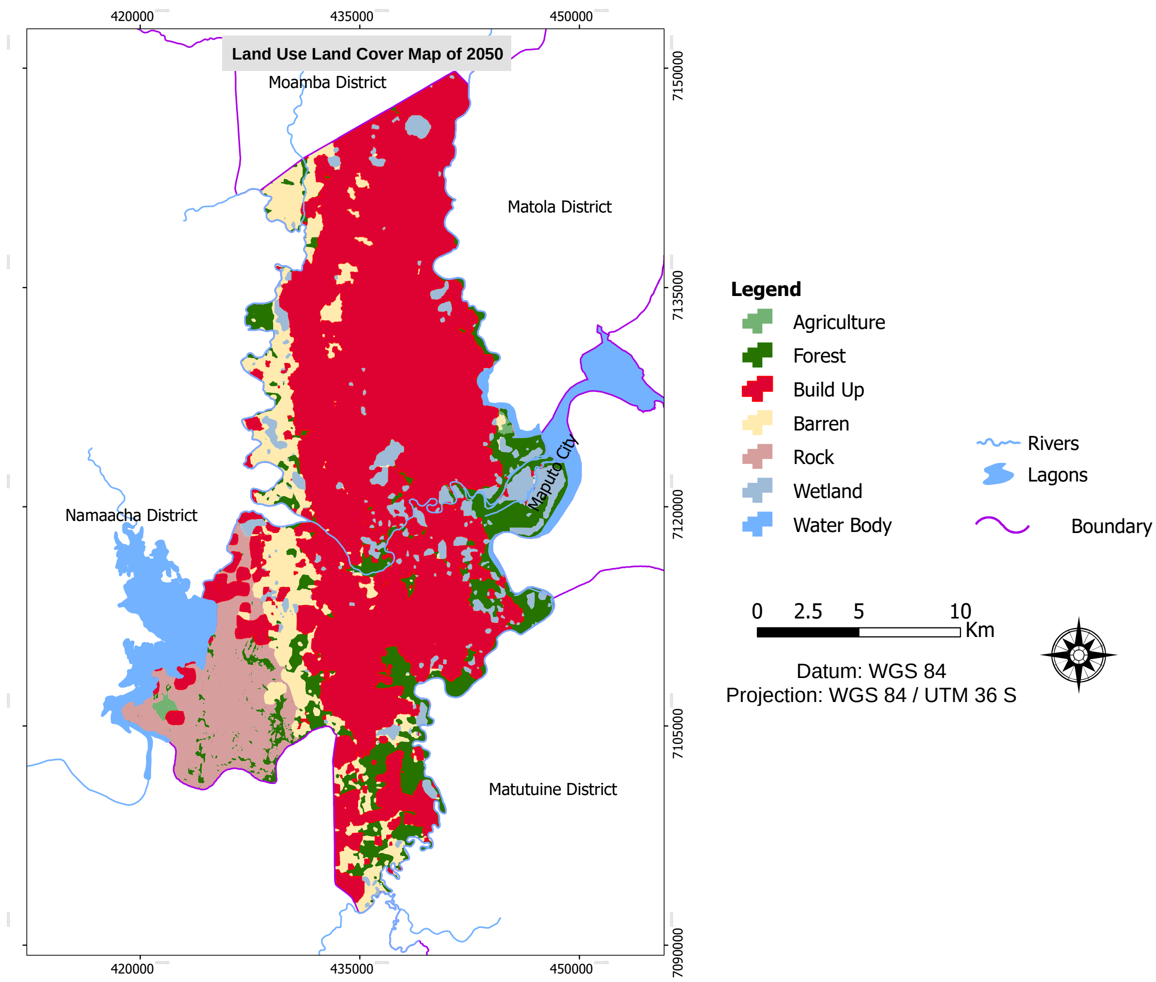

Figure 12. Map derived from the Cellular Automata-Markov chain model, predicting future land use land cover scenarios for 2050

Between 2020 and 2050, the build-up class will gain area mainly from forest, barren, rock and wetlands classes, with a total of 52.15 Sq.km, 50.96 Sq.km, 17.75 Sq.km and 14.14 Sq.km, respectively (Table 24; Figure 12). This class will have 345 Sq.km of unchanged area. In contrast, forest, will lose total area by converting to baren lands and wetlands by 9.50 Sq.km and 4.95 Sq.km. The persistence area will be 78.64 Sq.km.

Barren will lose 5.84 Sq.km and 3.55 Sq.km to forest and wetlands, respectively, while rock will lose 8.06 Sq.km to barren, 1.44 Sq.km to wetlands and 1.05 Sq.km to forest. Wetland area will reduce by converting to forest and barren lands by 4.83 Sq.km and 2.59 Sq.km, respectively, as the most representative.

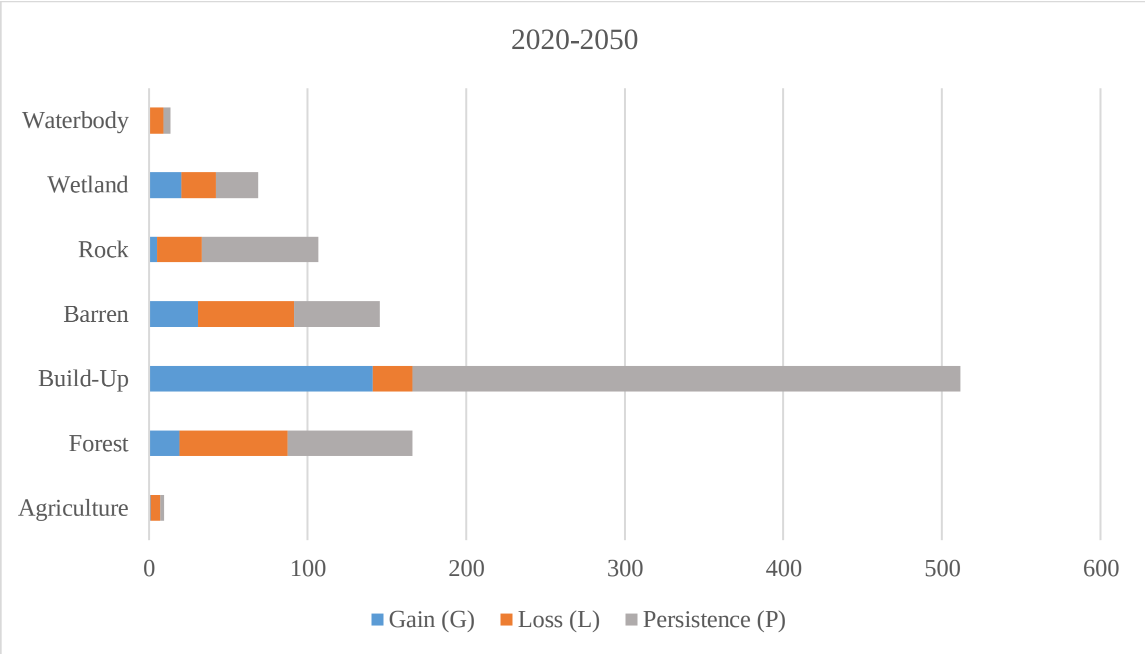

Figure 13. Land use land cover quantitative information (gains, loss and persistence) within each class and between 2020 and 20250

Table 23. Output of long-term change analyse comparing 30 years, showing values of persistence, gains and loss, swapping areas, changes and shares, between 2020 and 2050

Land use land cover class	Total		Persistence (P)	Gain (G)	Loss (L)	Swap (S)	Total Change	Absolute Net Change	Share of 2020	Share of 2050
	2020	2050								
Agriculture	8.28	3.27	2.1	1.08	6.16	7.24	7.24	-0.01	0.01	0.00
Forest	147.20	97.79	78.6	19.06	68.24	87.36	87.30	-0.06	0.18	0.12
Build-up	370.78	487.10	345.8	141.10	24.82	165.78	165.93	0.14	0.46	0.61
Barren	114.91	85.36	54.4	30.89	60.42	91.34	91.30	-0.04	0.14	0.11
Rock	101.75	78.34	73.3	4.96	28.34	33.33	33.30	-0.03	0.13	0.10
Wetland	48.31	46.99	26.6	20.38	21.68	42.06	42.06	0.00	0.06	0.06
Waterbody	13.08	5.47	4.5	0.71	8.51	9.23	9.22	-0.01	0.02	0.01

The overall land changes in different periods (Figure 13) indicate that from 1984 to 1990, the study area experienced a total of 425.61 Sq.km of changes. Between 1990 and 2000, it was 467.69 Sq.km, 449.76 Sq.km from 2000-2010, 468.36 Sq.km from 2010-2020, and by 2050, it will be 295.81 Sq.km.

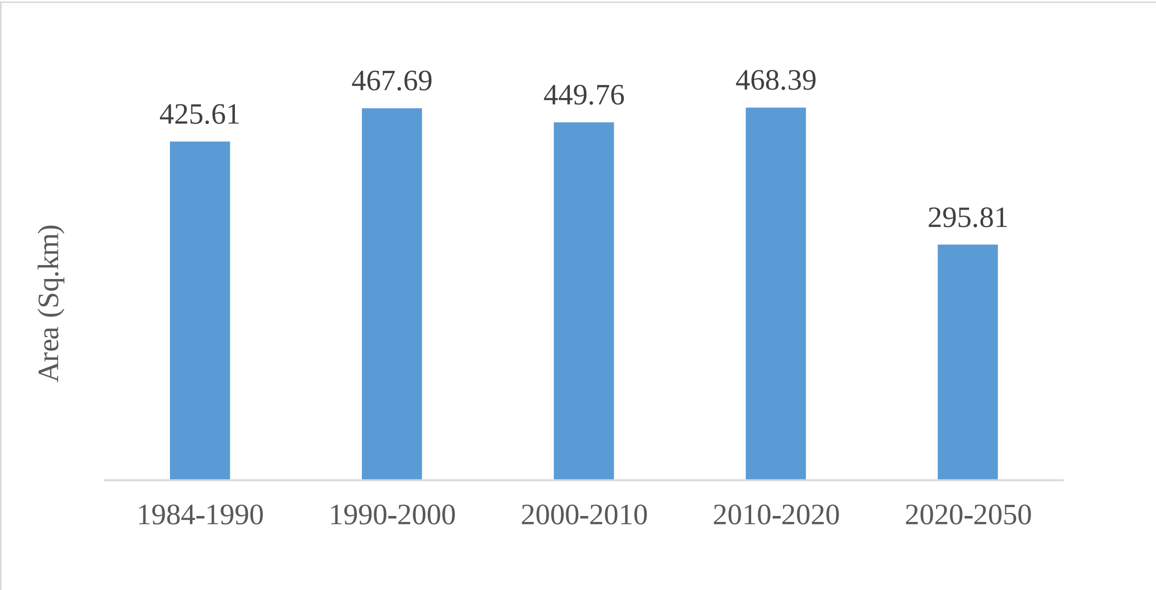

Figure 14. Total land use change and overall trend in different periods of the study

CHAPTER FIVE

5. DISCUSSION

Since no anthropological survey or fieldwork was conducted to assess the classification and driving forces of LULC, all discussions in this study were based on the analysis of RS statistics data, supported by a literature review supplemented with population data obtained from census and population projections surveys by the NSI.

5.1 Land Use Land Cover Mapping

The research was able to determine the extent and intensity of changes in LULC, mapping all dominant land cover types in the study area. Forest, which was the most significant (39.7%), continuously declined at an annual change rate of -1.5% over the course of the study period, ending as the second major class with 18.3% total land size share. Agriculture, the second most important class (27.1%), showed a similar but steady decline, with an annual change rate of -2.67%, ending with a 1% share.

In contrast, build-up which was the least significant class (0.3%) showed the greatest increase, ending as the most significant class (46.1%). This build-up increasing size was at the expense of forest and agricultural lands (Figure 10). This and has also been documented in similar research reports by Mazalo (2018), Matule et al. (2017), Jemuce (2016), and Dias (2015), all noting that Boane is undergoing an extensive urbanisation process, converting agricultural and forest land cover areas.

According to these researchers, the rapid urbanisation occurred as a result of population migration from Maputo and Matola City to near peri-urban and rural areas (Boane and Marracuene) since those cities were overcrowded and beyond their capacity to expand. Furthermore, a new industrial complex installed in Beluluane Industrial Park (Matola Rio) in early 2002 created new employment opportunities, increasing land demand for settlement. Most recently, the construction of the Maputo-Catembe bridge (Maputo City) contributed significantly to a rapid increase in the population since it created a resettlement process for the households from the affected area in Boane.

This research is of the view that destroying areas that were once forests will affect the micro-climate, resulting in thermal variation, urban heat stress, oxygen deficiency, pollution, soil instability through erosion and increased flooding events if no measures are put in place to halt this urban sprawl. Similar was concluded by Halder et al. (2021) when assessing the impacts of urban expansion on land transformation in the West Bengal district, India

Moreover, converting agricultural lands into build-up will decrease the availability of food harvesting areas. According to Ndava et al. (2021), 74.5% of the productive area in Boane is used for rainfed agriculture by the familiar sector, which produces food crops for subsistence and drives the rural economy. The remaining 11.6% of the productive area is used in small-scale irrigation farming for commercial purposes, feeding mainly markets in the major cities (Maputo and Matola) and surroundings (State Administration Ministry, n.d). This will increase food insecurity in local markets and nearby major cities that heavily rely on these agricultural products.

On the other hand, although earth observation data have been intensively used in mapping LULC, one key limitation is cloud cover, especially for tropical countries influenced by an extensive precipitation regime throughout the year. For this research, it was of the utmost importance to obtain non-contaminated images from the wet season. Despite that, there were no images from the wet season with the same acquisition date and with cloud-free status conditions. Therefore, images from the end of the dry season and the beginning of the wet season were used. As a consequence, the forests, agriculture and wetlands classes were susceptible to being misclassified due to a similar visual spectrum when sampling, leading to confusion in the spectral pattern.

Macarringue et al. (2022) and Matule and Macarringue (2020) denoted similar problems assessing LULC in dispersed settlements with spontaneous occupation characteristics, with few or non-zoning plans, and low reflectance house roofs made of straw, grass, sticks and stakes, as providing a similar visual spectrum with barren and rock when sampling. Also, classifying the type of agriculture (rainfed) practised by the majority of households, which does not tend to be as concentrated as plantations, coupled with a high rate of vegetation removal, as a consequence of most spectral feature variability between LULC classes.

All these physical aspects may have led to the misclassification of feature objects in earth observation data with medium resolution (freely available), which are mostly used in developing countries such as Mozambique, and ultimately the LULC classification. As a consequence, the variability in most LULC classes, including build-up and barren, rocky and barren, wetland and waterbody, and forest with agriculture classes, can therefore be explained by excessive generalisation during data sampling rather than the algorithm selected.

Other drawbacks when mapping LULC are vegetation cover, soil moisture and image quality, which are greatly affected by the sensor's parameters and atmospheric conditions or pollution (Tibebe et al., 2020). Regarding vegetation cover, earth observation data has a good response when vegetation is phenological healthy, therefore, it is important to have images of the wet season because they display the best spectral variability between most LULCs (Tibebe et al., 2020).

5.1 Accuracy Assessment and Kappa Coefficient

This research mapped with highly accurate values despite the fact that some earth observation data, were difficult to use due to quality problems. Since 1980 was missing from the Landsat collection, data from 1984 (TM) was used which had poor spectral quality and spatial resolution (60 m). Moreover, image quality for 2010 was affected by a general gap line error caused by sensor (ETM+) failure. However, the overall accuracy was between 87% and 91%, with a kappa coefficient of 0.84 to 0.89, respectively. For user and producer accuracy, values were between an average of 89% to 90%, which according to the straightness of agreement is an acceptable result.

Using a similar method, Oliveira et al., (2019) reached 76.23% LULC accuracy mapping at the national scale (Mozambique). Similarly, Macarringue (2022) achieved 80.93% accuracy and a 0.880 kappa coefficient when regionally mapping the northern part of Mozambique. Other researchers, such as Gudo et al., (2022) achieved an average accuracy of 93.12% and a 0.9 kappa coefficient when analysing LULC changes for spatio-temporal dynamics in South Sudan. Furthermore, Zvobgo and Tsoka (2021) averaged 91.25% accuracy (0.89 kappa coefficient) when assessing the causes of deforestation in Zimbabwe. Schulz et al., (2021) achieved 73.3% accuracy mapping land use in a heterogeneous landscape of Sahel (Niger), indicating the robustness of the algorithm used for classifying LULC.

Other researchers that have used traditional optical mosaic data and maximum likelihood classification, such as Macarringue et al. (2019), who achieved 68% accuracy and a kappa coefficient of 0.6, and Mazalo (2018) recorded an average accuracy of 63.5% and a kappa coefficient of 0.697, showing that this algorithm cannot reliably estimate LULC in high diversity environments, compared to the new compositing techniques, spectral and temporal metrics and machine learning classification algorithms.

Using overall accuracy and the kappa coefficient as statistical metrics to validate LULC classification, the results of the current study were confirmed to be most close to reality, therefore, reliable. Analysing the performance of the classifier, the results were above the expected threshold for overall accuracy and kappa coefficient, with an average of 90% and 0.88, respectively, indicating very good agreement between the model used to predict and the classification process.

Comparing selected classes, waterbody was the easiest to map as it is a unique and special characteristics on earth without high reflectance values, and generally are dark on imagery. Therefore, user and producer accuracy of this class were always between 90 and 100%, during the classification process. Other classes presented a user and producer accuracy between 50% to 80%, which is moderate to good accuracy, observed mostly between forest and agriculture, agriculture and barren land, barren land and build-up, rock and barren land, and wetland and waterbody, and vice-versa, as they have similar spectral resolution characteristics.

The accuracy assessment is a statistical measure that gives confidence to the map user in classification, since it indicates how well the classification was performed comparatively to just random (Aburas et al., 2016).

5.2 Land Transformation

Using change detection, a fundamental step in the post-classification analysis, to inspect changes in LULC and attribute them to a specific cause, metrics of persistence, gains and loss, and swap were extracted, from which the main land transformation was derived. From the LULC pattern (Figure 5) initially characterised by extensive and uniform vegetation distribution, mostly covered by forest and agricultural (1984), construction (build-up) hugely increased and spread all over the study area (2020).

Consistent with values of persistence (unchanged area), built-up only changed 0.03%, while agriculture (12%) and forest (44%) changed the most. Supported by previous knowledge, urban areas don't transit to other class unless is observed a catastrophic event. Thus, in 2000 the study area was affected by cyclone Eline, with catastrophic floods being observed in the southern part of Mozambique, which may be responsible for this change, or can be seen as result of misclassified pixels during the classification process (Tibebe et al., 2020; Mondlhane, 2005; Pereira and Gonçalves, 2004; Cosgrave, 2001). Accordingly, the population grew at average rate of 4.57% (National Statistical Institute, n.d.) supporting the evidence that the study area is experiencing an urban sprawl.

Specifically, between 1984 and 1990, the pattern of LULC was mostly forest from the north to the south part of the study areas, and an agricultural fringe crossing from central east to the south-west part. According to the national reforestation strategy (2006) by the Ministry of Agriculture, between 1980-1987, the government which was a state-own enterprise, adopted initiatives of crop fast-growing forest species, supplying firewood and charcoal, to mitigate the pressure on the native forest by populations in major cities and surrounding areas. Under this initiative were cropped millions of hectares of Eucalyptus species, which doubled the country's forest area from 20000 ha to 42 000 ha in almost 20 years.

During this period, changes in agriculture land size account for -5.36%, while forest increased by 4.47 %, and presenting the highest persistence value (55%) which indicate that it continues to be the most significant class. From the change direction matrix, it was evident that between forest, agriculture, barren and wetland, there was an intense interchangeable pattern (all classes giving area to others), i.e., large areas of agriculture being converted to forest (78.4 Sq.km) and wetlands (34.2 Sq.km), barren being converted to agriculture (46.35 Sq.km), and forest to wetland (36.95 Sq.km). This is clear evidence of some misclassification between these classes due to a similar spectral resolution in medium earth observation data.

A small and concentrated settlements area was observed near and surrounding the main village (central part) and peri-urban area (north-east), a relatively secure area due to the civil war in the country displacing families and limiting their movement. Mussagy and BigramoAllaro (2016), in their before and after-war economic research report, also indicated this evidence, as well as population data (National Statistical Institute, n.d.) that shows an average growth of only 0.26%, equal to the average growth rate of the country.

From 1990 to 2000, forest started to decrease although showing the highest persistence value (50%). This scenario can be analysed as a consequence of the ending reforestation project near 1990 due to structural economic and political changes, with the launch of the first government five-year Economic Rehabilitation Programme (1987) aiming to privatise state-owned enterprises, and the emerging land demand due to a stable environment with the signing of the peace agreement in 1992, ending the civil war, which subsequently created a great movement from rural to urban areas triggered by new job opportunities in commerce and agriculture farms (Cruz et al., 2020; Mussagy and BigramoAllaro, 2016).

Population data (National Statistical Institute, n.d.) also indicates a large change (4.21%), which can explain the increase in agricultural area, as well as the build-up and barren land, because of this fast-growing demand in land for food production and housing. During this period, build-up showed an increasing pattern, spreading from the central part and covering a small fringe that goes from north-east to south-east, and mostly concentrated in the central part.

As of 2000 and 2010, statistical metrics indicates that forest had the highest total change area, accounting for 32% of the total lost area, mostly by conversion to barren (56.5 Sq.km). Although it continues to show the highest persistence value (41%), remaining significant. Agriculture, with a low persistence value (7%), started to decrease mainly by conversion to barren (56.5 Sq.km), thus, being the class with the largest lost area (34%) and the most changed area.

Conversely, barren with 8% persistence, increased the most (35% of the gain area). This increase can be understood as being caused by natural events, as there was a significant flood event in early 2000 (Cosgrave, 2001; Jury and Lucio, 2004), which was responsible for destroying large areas of agricultural cultures, as well as forest areas that are mainly constituted by fragile savannahs. On the other hand, Balas et al. (2021), Jemuce (2016) and Mussagy and BigramoAllaro (2016) considered this period remarkable because is marked by the establishment of the first mega-industrial project (2000) in Mozambique, introducing several industries, demanding and creating numerous employment and business opportunities.

This is also observed from the population data (National Statistical Institute, n.d.), which almost reaches 6.82% of annual average growth. This is linked to forest and agriculture conversion, meaning that those classes were destroyed. During this period, build-up increased at the expense of barren land (31.29 Sq.km) which have received areas mostly by conversion of agricultural and forest lands, covering the northern part down to the south.

From 2010 to 2020, direction of metrics data indicates that construction (build-up) hugely increased, accounting for 57% of the gain area, which is consistent with the high persistence value (31%), indicating that the unchanged area was greater. The pattern of LULC changed, spreading across the study area (all directions), to areas that were covered by barren lands (115.5 Sq.km), forest (109.8 Sq.km), and wetlands (22.9 Sq.km) in the past. Accordingly, the population grew at an average rate of 6.98% (National Statistical Institute, n.d.), supporting the evidence that the study area is experiencing urban sprawling.

Other population parameters (National Statistical Institute, n.d.), such as density, also indicates a huge change over the last 40 years, from 48 inhabitants per Sq.km in 1980 to 298 inhabitants per Sq.km in 2020, and is expected to increase more by 2050 to a total of 699 inhabitants per Sq.km. This rapid increase will demand more land for settlement, food generation and other human activities. As can be observed, during the study period (40 years) the population grew almost ten times more, which allies with traditional rules of land ownership, informal and disperse occupation characteristics, challenging the efforts for effective policing.

This study identified rapid population growth, urbanisation expansion and reduced vegetation cover as the primary factors affecting the LULC.

5.3 Land Cover Future Prediction

According to Aburas et al. (2016), simulation accuracy depends on several factors, including image quality, processing methods, data types, algorithm efficiency and factors influencing the land cover patterns (drivers). Unfortunately, most of these factors were beyond the control of the map maker. For example, the Landsat ETM+ (2010) image used to produce the 2020 predicted maps and validate the forecast process, presented a gap error due to a satellite general failure.

Therefore, it's believed that during the gap fill process, this image lost some quality, affecting the final prediction accuracy. Additionally, slope, population density and immigration, which were referred to as drivers of land transformation, in the study area were not taken into account in the simulation process. As seen in a study by Gharaibeh et al. (2020), a gentle slope is significantly attractive for land use change. Therefore, places with a low percentage of slope grow more easily, expected to be overfit by construction. The same can be deduced from the uncontrolled population growth and immigration, which significantly impacts land pressure, allied with the absence of policies and land use plans, that could be another alarming factor for the future of land use.

However, the CA-MC model used in this study performed well with two historic datasets, with an overall average of 86% accuracy. The validation results suggested very good agreement between the actual and the projected maps. This result is in accordance with other studies that used the same model. Merhej et al. (2022) achieved an accuracy of 79.3% when predicting LULC changes. Meanwhile, Gemmechis (2022), assessing the dynamics of LULC changes, achieved accuracy values above 80%. The same was achieved by Liping et al. (2018) when monitoring and predicting LULC changes.

Some studies achieved much higher accuracy with CA-MC models by improving the model by integrating other quantitative models, such as artificial neural networks, used to model complex patterns and behaviours (Gharaibeh et al., 2020). Asadi et al. (2022), simulating urban sprawling, achieved values of kappa Index of Agreement of 96.4% by integrating artificial neural networks.

Despite, this study only used few data sets (two classified images), other studies have demonstrated that the land use cover has a complex pattern. These approaches have proven that for realistic simulation of the future, driving forces, such as socio-economic, physical-natural and environmental factors, must be considered as inputs. If that is not the case, combining CA-MC with the other models that have these aspects can improve the simulation accuracy (Aburas et al., 2016).

CHAPTER SIX

6. CONCLUSION

By combining the most precise and accurate RS data from Landsat sensors, a machine learning classifier (RF), and CA-MC predictor model, the LULC of Boane was successfully mapped for the years 1984, 1990, 2000, 2010 and 2020, and forecasted for 2050.

Through a supervised process, seven land classes, i.e., agriculture, forest, build-up, barren, rock, wetlands and waterbody, were extracted and classified as the most observed in the study area. According to the results, build-up, barren, rock and waterbody increased by 45%, 3.4%, 1.9% and 0.5% in total size area, while agriculture, forest and wetland decreased by 26.1%, 21.4%, and 4.1%, respectively.

Other statistical data indicates that there was an alternance pattern of LULC between all land classes, with significant changes being observed for agriculture, forest and build-up. While agriculture and forest show a continuously decreasing pattern, the build-up class increased tremendously, as a result of a large population increase in this area and related human activities.

The classifier statistics for validation indicate an average threshold of 90% of accuracy assessment and a 0.8779 kappa coefficient, which indicates very good agreement between the model and classifier process, compared to randomly assigning values.

The conversion of large areas of forest and agriculture to build-up indicates their degradation or destruction to increase space to settlements or other human activities. The same can be concluded about baren, rocks and wetland areas, which increased between 1984 and 2020, indicating that these areas were cleaned in favour of build-up or settlements.

The direct impact of removing vegetation cover is increasing the earth's surface temperature, changing the precipitation regime and water cycle. By increasing surface temperature, conditions of flood events are created in rainfall seasons. Uncontrolled flooding will increase soil erosion with other ecological consequences that will likely affect the micro-climate.

This study clearly indicates that a fast-growing population has significant impacts on LULC over time for land management planning and the environmental ecosystem. An increasing population strongly relies on land for settlements and food production, reducing the land cover protecting the earth's surface, increasing temperature, erosion, and affecting the water cycle and other environmental issues (Faye et al., 2022).

The forecast results indicate that all classes are expected to change, but build-up will continue to be the significant class in Boane by 2050. The results of the prediction model indicate that build-up will account for 60% of the total area, if the management conditions remain as of 2020. The remain classes will continue to decrease following the current pattern.

From this finding, one can conclude that the LULC situation in the next 30 years will be critical if no action is taken to stop this uncontrolled urban sprawling. Adequate land use planning must be developed with clear indications of location for different activities or human uses, with a clear plan of action to implement this guidance to revert this fast urban expansion.

By studying these outcomes further, one is informed of land use change patterns, and land use change behaviours and change speed. This important information would be very helpful for urban planners and decision-makers.

The results obtained in this research attest that the methodology and the process are valid. This study can be replicated in all growing districts of Mozambique as an important tool for suitable land cover planning, as it is less costly and time-consuming. To enhance the ability of the model to predict future land cover changes, more factors must be considered, which will improve the understanding of the land cover processes.

6.1 Limitations of the Research

Data may contain flaws, errors or uncertainty that affect results and methodology, so this study may have some limitations. Therefore, for further improvement of the classification process:

a) High-resolution images are required for a more detailed analysis of mixed pixels, i.e., pixels that are present in two or more classes, which may lead to a misclassification of a specific land class;

b) Variables with significant impact in analysing, classifying, and predicting spectral data (influential spectral variables) must be identified and considered when calibrating the model to improve the overall efficiency and accuracy;

c) In order to maximize the overall performance and minimize errors and inaccurate outputs, optimal values for each hyperparameter must be set (turned) before running the model (RF);

d) Although historical google earth images with high resolution had been used to visually correct the sampling process, ground truth data should be collected whenever possible;

e) This research focused on analysing land transformation from a perspective of changes that occurred in the area of study area, mapping LULC, detecting the directions and extent of changes between land cover classes, and identifying the driving factors and their correlation with changes in LULC. To have a complete overview of land transformation, complementary studies of land suitability and water availability must be undertaken to have a land management plan;

f) Although the potential of the CA-MC method has been recognised by previous studies, a realistic simulation needs to be performed taking into account social, environmental and economic driving forces. Therefore, the CA-MC model can be integrated with other models to obtain a better understanding of changing, growth patterns and to improve the model's prediction capability.

References

Aburas, M. M., Ho, Y. M., Ramli, M. F., & Ash'aari, Z. H. (2016). The simulation and prediction of spatio-temporal urban growth trends using cellular automata models: A review. *International Journal of Applied Earth Observation and Geoinformation*, 52, 380–389. https://doi.org/10.1016/j.jag.2016.07.007

Ali, U., Esau, T. J., Farooque, A. A., Zaman, Q. U., Abbas, F., & Bilodeau, M. F. (2022). Limiting the collection of ground truth data for land use and land cover maps with machine learning algorithms. *ISPRS International Journal of Geo-Information*, 11(6), Article 6. https://doi.org/10.3390/ijgi11060333

Al-Khaqani, E.T., & Al- Ruwashdi, M.F. (2022). Simulating and predicting of urban expansion in Al Najaf City utilizing a CA-Markov model. Presented at the AIP Conference Proceedings: Third Annual Conference of Al-Muthanna University/College of Science, Iraq. https://doi.org/10.1063/5.0094462

Alshari, E., & Gawali, B. (2022). Modeling land use change in Sana'a city of Yemen with Molusce. *Journal of Sensors*, 7419031, 1–15. https://doi.org/10.1155/2022/7419031

Al-sharif, A., & Pradhan, B. (2013). Monitoring and predicting land use change in Tripoli Metropolitan City using an integrated Markov chain and cellular automata models in GIS. *Arabian Journal of Geosciences*, 7, 1–11. https://doi.org/10.1007/s12517-013-1119-7

Ameja, L., Ribeiro, N., & Sitoe, A. (2022). Land use and land cover changes of Gile national park buffer zone from 1999 to 2019, Central Mozambique. *American-Eurasian Journal of Agricultural & Environmental Sciences,* 21, 39-52, https://doi.org/10.5829/idosi.aejaes.2021.39.52

Amin, A., & Fazal, S. (2012). Land transformation analysis using remote sensing and GIS techniques (A case study). *Journal of Geographic Information System*, 04(03), 229–236. https://doi.org/10.4236/jgis.2012.43027

Aquino, A., Lim, C., Kaechele, K., & Taquidir, M. 2018. *Mozambique Country Forestry Note (Policy Note).* World Bank, Washington, DC. https://doi.org/10.1596/30935

Asadi, M., Oshnooei-Nooshabadi, A., Saleh, S., Habibnezhad, F., Sarafraz Asbagh, S., & van Genderen, J. (2022). Simulation of urban sprawl by comparison cellular automata-Markov and ANN. Environmental and Earth Sciences, Environmental Science, 2022080119, 1-14. https://doi.org/10.20944/preprints202208.0119.v1

Ashish, D., & McClendon, R. (2009). Land-use classification of multispectral aerial images using artificial neural networks. *International Journal of Remote Sensing*, 30, 1989–2004. https://doi.org/10.1080/01431160802549187

Avtar, R., Komolafe, A. A., Kouser, A., Singh, D., Yunus, A. P., Dou, J., Kumar, P., Gupta, R. D., Johnson, B. A., Thu Minh, H. V., Aggarwal, A. K., & Kurniawan, T. A. (2020). Assessing sustainable development prospects through remote sensing: A review. *Remote Sensing Applications: Society and Environment*, 20, 100402. https://doi.org/10.1016/j.rsase.2020.100402

Awuh, M. E., Japhets, P. O., Officha, M. C., Okolie, A. O., & Enete, I. C. (2019). A correlation analysis of the relationship between land use and land cover/land surface temperature in Abuja Municipal, FCT, Nigeria. *Journal of Geographic Information System*, 11(1), Article 1. https://doi.org/10.4236/jgis.2019.111004

Azizi, A., Malakmohamadi, B., & Jafari, H. R. (2016). Land use and land cover spatiotemporal dynamic pattern and predicting changes using integrated CA-Markov model. *Global Journal of Environmental Science and Management*, 2, 223-234. https://doi.org/10.7508/gjesm.2016.03.002

Bagarinao, R., Khouangvichit, P., Pacardo, E., & Rebancos, C. (2020). Assessment of land use and land cover change in Dong Na Tard provincial protected area, Savannakhet Province, Lao PDR. *International Journal of Advanced Research and Publications,* 4(3), 115–120.

Balas, M., Carrilho, J., & Lemmen, C. (2021). The fit for purpose land administration approach-connecting people, processes and technology in Mozambique. *Land*, 10, 1-22. https://doi.org/10.3390/land10080818

Barsi, J., Markham, B., Czapla-Myers, J., Helder, D., Hook, S., Schott, J., & Haque, M. O. (2016). Landsat-7 ETM+ radiometric calibration status. In Proceedings of SPIE--*The*

International Society for Optical Engineering, 9972, 1-24. https://doi.org/10.1117/12.2238625

Bayas, S., Sawant, S., Dhondge, I., Kankal, P., & Joshi, A. (2022). Land use land cover classification using different ML algorithms on Sentinel-2 Imagery. In: Gupta, D., Sambyo, K., Prasad, M., & Agarwal, S. (eds) Advanced machine intelligence and signal processing. Lecture notes in electrical engineering. *Springer*, 858, 761–777. https://doi.org/10.1007/978-981-19-0840-8_59

Bell, T. W., Allen, J. G., Cavanaugh, K. C., & Siegel, D. A. (2020). Three decades of variability in California's giant kelp forests from the Landsat satellites. *Remote Sensing of Environment*, 238, 110811. https://doi.org/10.1016/j.rse.2018.06.039

Bernales, A. M., Antolihao, J., Samonte, C., Campomanes, F., Rojas, R., & Silapan, J. (2016). Modelling the relationship between land surface temperature and landscape patterns of land use land cover classification using multi linear regression models. *International Archives of the Photogrammetry, Remote Sensing and Spatial Information Sciences*, XLI-B8, 851–856. https://doi.org/10.5194/isprsarchives-XLI-B8-851-2016

Bhatta, B. (2013). *Research Methods in Remote Sensing*. Springer Briefs in Earth Sciences, Series E-ISSN: 2191-5377, Springer Dordrecht Heidelberg New York London, UK. https://doi.org/10.1007/978-94-007-6594-8

Bilolikar, D., More, A., Gong, A., & Janssen, J. (2023). How to out-perform default random forest regression: Choosing hyperparameters for applications in large-sample hydrology. *In press*. https://doi.org/10.48550/arXiv.2305.07136

Boane / Perfis Distritais / A Província / Início—Portal do Governo da Provincia de Maputo. (State Administration Ministry n.d.). Retrieved July 6, 2022, from https://www.pmaputo.gov.mz/por/A-Provincia/Perfis-Distritais/Boane

Calderón-Loor, M., Hadjikakou, M., & Bryan, B. A. (2021). High-resolution wall-to-wall land-cover mapping and land change assessment for Australia from 1985 to 2015. *Remote Sensing of Environment*, 252, 112148. https://doi.org/10.1016/j.rse.2020.112148

Carcausto, S. E., Pricope, N., Vargas-Machuca, D., Huanca, O., & Naupari, J. (2022). Mapping land cover types for highland Andean ecosystems in Peru using google earth engine. *Remote Sensing*, 14, 1562. https://doi.org/10.3390/rs14071562

Chakraborty, S., Majumdar, D., & Sahoo, S. (2013). Comparative analysis of different supervised classification techniques using linear regression model. *ZENITH International Journal of Multidisciplinary Research*, 3(7), 317-327.

Chel, S. (2023). Population growth and socio economic condition of people. *Journal of Social Studies: Economy, Polity, Environment*, 3(2), 1–15.

Chen, Y., Hou, J., Huang, C., Zhang, Y., & Li, X. (2021). Mapping maize area in heterogeneous agricultural landscape with multi-temporal Sentinel-1 and Sentinel-2 images based on random forest. *Remote Sensing*, 13(15) 2988. https://doi.org/10.3390/rs13152988

Chughtai, A. H., Abbasi, H., & Karas, I. R. (2021). A review on change detection method and accuracy assessment for land use land cover. *Remote Sensing Applications: Society and Environment*, 22, 100482. https://doi.org/10.1016/j.rsase.2021.100482

Cosgrave, J. (2001). Mozambique and the great flood of 2000. *Journal of Refugee Studies*, 14, 452–453. https://doi.org/10.1093/jrs/14.4.452

Cruz, A. S., Ferreira, I. A., Flentø, J., Jones, S., & Tarp, F. (2020). *Historical, political, and economic background. In Economic Development and Institutions – Mozambique at a Fork in the Road*: An Institutional Diagnostic [Draft report]. UNU WIDER.

Czekajlo, A., Coops, N. C., Wulder, M. A., Hermosilla, T., White, J. C., & van den Bosch, M. (2021). Mapping dynamic peri-urban land use transitions across Canada using Landsat time series: Spatial and temporal trends and associations with socio-demographic factors. *Computers, Environment and Urban Systems*, 88, 101653. https://doi.org/10.1016/j.compenvurbsys.2021.101653

Dessu, T., Korecha, D., Hunde, D., & Worku, A. (2020). Long-term land use land cover change in urban centers of southwest Ethiopia from a climate change perspective. *Frontiers in Climate*, 2. 577169. https://doi.org/10.3389/fclim.2020.577169

Dias, C. M. M. T. (2015). Análise espacial do uso e cobertura da terra em Moçambique: Análise espacial da evolução do uso e cobertura da terra em Moçambique. Master Theses, Pontifica Universidade Católica de Minas Gerais, Belo Horizonte, Brasil.

Digra, A., & Kaushal, A. (2021). Land use and land cover change analysis using remote sensing and gis techniques. *Biological Forum – An International Journal*, 13(3b), 134-138.

Dissani, B. M., Ayenagbo, K., & N'Souvi, K. (2021). The impact of deforestation on co2 emissions: evidence from WAEMU. *International Journal of Science and Business*, 5, 75-87

Erdem, F., Atun, R., Yigit Avdan, Z., Atila, I., & Avdan, U. (2021). Drought analysis of Van Lake basin with remote sensing and GIS technologies. *The Egyptian Journal of Remote Sensing and Space Science*, 24(3), 1093–1102. https://doi.org/10.1016/j.ejrs.2021.10.006

Faye, B., Du, G., & Zhang, R. (2022). Efficiency analysis of land use and the degree of coupling link between population growth and global built-up area in the subregion of West Africa. *Land*, 11(6), 847. https://doi.org/10.3390/land11060847

Fokeng, R. M., Forje, W. G., Meli, V., & Bodzemo, B. N. (2020). Multi-temporal forest cover change detection in the Metchie-Ngoum protection forest reserve, West Region of Cameroon. *The Egyptian Journal of Remote Sensing and Space Science*, 23(1), 113–124. https://doi.org/10.1016/j.ejrs.2018.12.002

Gao, H., & Song, W. (2022). Assessing the landscape ecological risks of land-use change. *International Journal of Environmental Research and Public Health*, 19(21), 13945. https://doi.org/10.3390/ijerph192113945

Gaur, S., Mittal, A., Bandyopadhyay, A., Holman, I., & Singh, R. (2020). Spatio-temporal analysis of land use and land cover change: A systematic model inter-comparison driven by integrated modelling techniques. *International Journal of Remote Sensing*, 41(23), 9229–9255. https://doi.org/10.1080/01431161.2020.1815890

Gemmechis, W. A. (2022). Modeling earth systems and environment land use land cover dynamics using CA-Markov chain model and geospatial techniques: A case of Belete

Gera regional forest priority area, South Western Ethiopia. *Research Square*, 1, 1-23. https://doi.org/10.21203/rs.3.rs-2129572/v1

Gharaibeh, A., Shaamala, A., Obeidat, R., & Al-Kofahi, S. (2020). Improving land-use change modeling by integrating ANN with cellular automata-Markov chain model. *Heliyon*, 6 (9), 1-18. https://doi.org/10.1016/j.heliyon.2020.e05092

Gilani, H., Naz, H. I., Arshad, M., Nazim, K., Akram, U., Abrar, A., & Asif, M. (2021). Evaluating mangrove conservation and sustainability through spatiotemporal (1990–2020) mangrove cover change analysis in Pakistan. *Estuarine, Coastal and Shelf Science*, 249, 107128. https://doi.org/10.1016/j.ecss.2020.107128

Giordano, F., & Marini, A. (2008). A landscape approach for detecting and assessing changes in an area prone to desertification in Sardinia (Italy). *International Journal of Navigation and Observation*, 1-7, 549630. https://doi.org/10.1155/2008/549630

Gonçalves, R., & Assis, L. (2007). Comparison of sampling methods to classification of remotely sensed images. IV Simpósio Internacional de Agricultura de Precisão, 1-4 Minas Gerais, Brasil.

Goswami, A., Sharma, D., Mathuku, H., Gangadharan, S. M. P., Yadav, C. S., Sahu, S. K., Pradhan, M. K., Singh, J., & Imran, H. (2022). Change detection in remote sensing image data comparing algebraic and machine learning methods. *Electronics*, 11(3), 431. https://doi.org/10.3390/electronics11030431

Gudo, A. J. A., Deng, J., & Qureshi, A. S. (2022). Analysis of spatiotemporal dynamics of land use/cover changes in Jubek State, South Sudan. *Sustainability*, 14(17), 10753. https://doi.org/10.3390/su141710753

Halder, B., Haghbin, M., & Farooque, A. (2021). An assessment of urban expansion impacts on land transformation of Rajpur-Sonarpur Municipality. *Knowledge-Based Engineering and Sciences*, 2(3), 34–53. https://doi.org/10.51526/kbes.2021.2.3.34-53

Hashim, M., Yahya, N., Ahmad, S., Komatsu, T., Misbari, S., & Md Reba, M. N. (2014). Determination of seagrass biomass at Merambong Shoal in straits of Johor using satellite remote sensing technique. *Malayan Nature Journal*, 66, 20–37.

Hassan, Z., Shabbir, R., Ahmad, S. S., Malik, A. H., Aziz, N., Butt, A., & Erum, S. (2016). Dynamics of land use and land cover change (LULCC) using geospatial techniques: A case study of Islamabad Pakistan. *Springer Plus, 5*(1), 812. https://doi.org/10.1186/s40064-016-2414-z

Herrmann, S., & Mohr, K. (2011). A continental-scale classification of rainfall seasonality regimes in Africa based on gridded precipitation and land surface temperature products. *Journal of Applied Meteorology and Climatology*, 50, 2504–2513. https://doi.org/10.1175/JAMC-D-11-024.1

Hua, A. K. (2017). Application of Ca-Markov model and land use/land cover changes in Malacca river watershed, Malaysia. *Applied Ecology and Environmental Research*, 15(4), 605–622. https://doi.org/10.15666/aeer/1504_605622

Huang, X., Wu, Z., Zhang, Q., & Cao, Z. (2022). How to measure wetland destruction and risk: Wetland damage index. *Ecological Indicators*, 141, 109126. https://doi.org/10.1016/j.ecolind.2022.109126

Jansen, L., & Di Gregorio, A. (2000). *Land cover classification system (LCCS): Classification concepts and user manual*. Food and Agriculture Organization of the United Nations, Rome, 1998

Jasim, M. A., Shafri, H. Z. M., Hamedianfar, A., & Sameen, M. I. (2016). Land transformation assessment using the integration of remote sensing and GIS techniques: A case study of Al-Anbar Province, Iraq. *Arabian Journal of Geosciences*, 9 (15), 667. https://doi.org/10.1007/s12517-016-2697-y

Jemuce, J. L. (2016). Gentrificação e urbanização extensiva: Caso do Distrito de Boane, Província de Maputo - Moçambique. Master Theses, Universidade Federal do Rio Grande do Sul, Brasil. https://lume.ufrgs.br/handle/10183/148307

Jhonnerie, R., Siregar, V. P., Nababan, B., Prasetyo, L. B., & Wouthuyzen, S. (2015). Random forest classification for mangrove land cover mapping using Landsat 5 TM and Alos Palsar imageries. *Procedia Environmental Sciences*, 24, 215–221. https://doi.org/10.1016/j.proenv.2015.03.028

Jombo, S., Adam, E., & Odindi, J. (2017). Quantification of landscape transformation due to the Fast Track Land Reform Programme (FTLRP) in Zimbabwe using remotely sensed data. *Land Use Policy*, 68, 287–294. https://doi.org/10.1016/j.landusepol.2017.07.023

Joshi, N., Baumann, M., Ehammer, A., Fensholt, R., Grogan, K., Hostert, P., Jepsen, M. R., Kuemmerle, T., Meyfroidt, P., Mitchard, E. T. A., Reiche, J., Ryan, C. M., & Waske, B. (2016). A review of the application of optical and radar remote sensing data fusion to land use mapping and monitoring. *Remote Sensing*, 8(1), 70. https://doi.org/10.3390/rs8010070

Kafy, A. A., Dey, N. N., Al Rakib, A., Rahaman, Z. A., Nasher, N. M. R., & Bhatt, A. (2021). Modeling the relationship between land use/land cover and land surface temperature in Dhaka, Bangladesh using CA-ANN algorithm. *Environmental Challenges*, 4, 100190. https://doi.org/10.1016/j.envc.2021.100190

Kattenborn, T., Leitloff, J., Schiefer, F., & Hinz, S. (2021). Review on convolutional neural networks (CNN) in vegetation remote sensing. *ISPRS Journal of Photogrammetry and Remote Sensing*, 173, 24–49. https://doi.org/10.1016/j.isprsjprs.2020.12.010

Kaur, M., Tur, N., Singh, A., Mehra, D., Singh, H., Devaser, V., & Kumar, R. (2012). Land transformation and urban sprawl mapping, using remote sensing and GIS technologies— A case study of Amritsar City, India. *Indian Journal of Ecology*, 39, 6–10.

Kesgin, B., & Nurlu, E. (2008). Land cover changes on the coastal zone of Candarli Bay, Turkey using remotely sensed data. *Environmental Monitoring and Assessment*, 157, 89–96. https://doi.org/10.1007/s10661-008-0517-x

Khan, T. (2017). Assessment of land use pattern in District Abbottabad through geographic information system and remote sensing. *Biologia (Lahore, Pakistan)*, 63, 87–96.

Kotaridis, I., & Lazaridou, M. (2021). Remote sensing image segmentation advances: A meta-analysis. *ISPRS Journal of Photogrammetry and Remote Sensing*, 173, 309–322. https://doi.org/10.1016/j.isprsjprs.2021.01.020

LaGro, J. A. (2005). *Land-use classification*. In D. Hillel (Ed.), Encyclopedia of Soils in the Environment, 321–328. https://doi.org/10.1016/B0-12-348530-4/00530-0

Lal, K., Kumar, D., & Kumar, A. (2017). Spatio-temporal landscape modeling of urban growth patterns in Dhanbad urban agglomeration, India using geoinformatics techniques. *The Egyptian Journal of Remote Sensing and Space Science*, 20(1), 91–102. https://doi.org/10.1016/j.ejrs.2017.01.003

Lambin, E., Geist, H., & Lepers, E. (2003). Dynamics of land-use and land-cover change in tropical regions. *Annual Review of Environment and Resources*, 20(49), 205-241.

Liping, C., Yujun, S., & Saeed, S. (2018). Monitoring and predicting land use and land cover changes using remote sensing and GIS techniques—A case study of a hilly area, Jiangle, China. *Plos one*, 13, 1-23. https://doi.org/10.1371/journal.pone.0200493

Liu, D., & Zhang, X. (2022). Occurrence prediction of pine wilt disease based on CA–Markov model. *Forests*, 13(10), 1-23. https://doi.org/10.3390/f13101736

Macarringue, L. S., Bolfe, É. L., & Pereira, P. R. M. (2022). Developments in land use and land cover classification techniques in remote sensing: A Review: *Journal of Geographic Information System*, 14(01), 1–28. https://doi.org/10.4236/jgis.2022.141001

Macarringue, L., Bolfe, É., & Fumo, Ó. (2020). Abordagens metodológicas no campo da dinâmica de uso e cobertura de terra: Um olhar para a realidade Moçambicana. *Geografia*, 45, 65–88. https://doi.org/10.5016/geografia.v45i1.14547

Macarringue, L., Matule, E., & Matumbuane, N. (2019). Integração da dimensão espacial na planificação de uso de terra ao nível distrital -estudo de caso de Boane. Conference: Simpósio brasileiro de sensoriamento remoto. https://doi.org/10.13140/RG.2.2.15017.34401

Majumdar, S. (2020). Assessment and detection of land cover changes in the southern fringe of Kolkata using remotely sensed data. *Geography, Environment, Sustainability*, 13(4), 1-12. https://doi.org/10.24057/2071-9388-2020-65

Manteigas, J. B. (2009). Potencialidade de imagem de satélite no monitoramento do uso e cobertura de terra, Distrito da Maganja da Costa, Zambezia, Mocambique. Master Theses, Universidade Eduardo Mondlane, Mozambique. http://monografias.uem.mz/handle/123456789/2054

Marzoli, A., n.d. *Avaliação integrada das florestas de Moçambique: Inventário Florestal Nacional.* Cooperação Italiana, Ministério de Agricultura, Maputo, Mozambique

Matule, E., & Macarringue, L. (2020). Avaliação da vulnerabilidade à perda de solo no distrito de Boane em Moçambique. *Sociedade & Natureza*, 32, 225–235. https://doi.org/10.14393/SN-v32-2020-46916

Matule, E., Ponzoni, F., & Chaves, J. (2017). Análise espaço-temporal dos índices de cobertura vegetal no município da Matola, Moçambique. *Sociedade & Natureza*, 29, 371–385. https://doi.org/10.14393/SN-v29n3-2017-1

Mazalo, E. da C. J. (2018). *Cartografia de ocupação da terra com imagens Landsat para o distrito de Marracuene—Moçambique*. Master Theses, Universidade Nova de Lisboa, Portugal. https://run.unl.pt/handle/10362/48103

Memarian, H., Balasundram, S. K., Talib, J. B., Sung, C. T. B., Sood, A. M., & Abbaspour, K. (2012). Validation of CA-Markov for Simulation of Land Use and Cover Change in the Langat Basin, Malaysia. *Journal of Geographic Information System*, 4(6), 1-13. https://doi.org/10.4236/jgis.2012.46059

Merhej, O., Ali, M., & Thabeet, A. (2022). Using CA-Markov model to predict land use/land cover changes in Bayer and Al-Bassit region, Latakia, Syria. *Journal of Agricultural and Marine Sciences*, 27(2), 50–58.

Mishra, V., Rai, P., & Mohan, K. (2014). Prediction of land use changes based on land change modeler (LCM) using remote sensing: A case study of Muzaffarpur (Bihar), India. *Journal of the Geographical Institute Jovan Cvijic, SASA*, 64(1), 111–127. https://doi.org/10.2298/IJGI1401111M

Mondal, Md. S., Sharma, N., Garg, P. K., & Kappas, M. (2016). Statistical independence test and validation of CA Markov land use land cover (LULC) prediction results. *The Egyptian Journal of Remote Sensing and Space Science*, 19(2), 259–272. https://doi.org/10.1016/j.ejrs.2016.08.001

Mondlhane, A. (2005). Integrated risk response techniques in emergence situations 1: "The Mozambique floods case simulations." In *Ecol. Environ*, 84, 1-10 https://doi.org/10.2495/SPD051162

Mucova, S. A. R., Filho, W. L., Azeiteiro, U. M., & Pereira, M. J. (2018). Assessment of land use and land cover changes from 1979 to 2017 and biodiversity & land management approach in Quirimbas National Park, Northern Mozambique, Africa. *Global Ecology and Conservation*, 16, 1-17. https://doi.org/10.1016/j.gecco.2018.e00447

Muhammad, R., Zhang, W., Abbas, Z., Guo, F., & Gwiazdzinski, L. (2022). Spatiotemporal change analysis and prediction of future land use and land cover changes using QGIS MOLUSCE plugin and remote sensing big data: A case study of Linyi, China. *Land*, 11(3), 419. https://doi.org/10.3390/land11030419

Musetsho, K. D., Chitakira, M., & Nel, W. (2021). Mapping land-use/land-cover change in a critical biodiversity area of South Africa. *International Journal of Environmental Research and Public Health*, 18(19), 1-14. https://doi.org/10.3390/ijerph181910164

Mussagy, I., & BigramoAllaro, H. (2016). Structural change in Mozambique: Economic performance before and after the civil war. *Journal of Economics and Sustainable Development*, 7, 119–125.

Nakamo, J., Wijaya, S., & Setiawan, Y. (2022). Assessment of land cover changes in Litumbandyosi-Gesimasowa game reserve using remote sensing and GIS. *IOP Conference Series: Earth and Environmental Science*, 950, 012083. https://doi.org/10.1088/1755-1315/950/1/012083

Nations, U. (n.d.). *Population*. United Nations. Retrieved May 18, 2022, from https://www.un.org/en/global-issues/population

Nguyen, H. A. T., Sophea, T., Gheewala, S. H., Rattanakom, R., Areerob, T., & Prueksakorn, K. (2021). Integrating remote sensing and machine learning into environmental monitoring and assessment of land use change. *Sustainable Production and Consumption*, 27, 1239–1254. https://doi.org/10.1016/j.spc.2021.02.025

Nkundabose, J. P., Nshimiyimana, F., Twagirayezu, G., & Irumva, O. (2021). Employing remote sensing tools for assessment of land use/land cover (LULC) changes in Eastern Province, Rwanda. *American Journal of Remote Sensing*, 9(1), 23-32. https://doi.org/10.11648/j.ajrs.20210901.13

Nugroho, A., Hasyim, A., & Usman, F. (2018). Urban growth modelling of Malang city using artificial neural network based on multi-temporal remote sensing. *Civil and Environmental Science*, 1(2), 052–061. https://doi.org/10.21776/ub.civense.2018.00102.2

Obaid, A., Adam, E., & Ali, K. A. (2023). Land use and land cover change in the Vaal Dam catchment, South Africa: A study based on remote sensing and time series analysis. *Geomatics*, 3(1), 205–220. https://doi.org/10.3390/geomatics3010011

Oliveira, W. N. D., Miziara, F., & Ferreira, N. C. (2019). Mapeamento do uso e cobertura do solo de Moçambique utilizando a plataforma google earth engine. *Anuário do Instituto de Geociências*, 42(1), 336-345. https://doi.org/10.11137/2019_1_336_345

Pereira, M., & Gonçalves, P. (2004). Effects of the 2000 southern Mozambique floods on a marginal coral community: The case at Xai-Xai. *African Journal of Aquatic Science*, 29, 113–116. https://doi.org/10.2989/16085910409503800

Population Projections 2017—2050—National Statistical Institute. (n.d.). Retrieved May 19, 2022, from http://www.ine.gov.mz/iv-rgph-2017/projeccoes-da-populacao-2017-2050

Probst, P., Wright, M. N., & Boulesteix, A.-L. (2019). Hyperparameters and tuning strategies for random forest. *WIREs Data Mining and Knowledge Discovery*, 9(3), e1301. https://doi.org/10.1002/widm.1301

Puig, C., Hyman, G., & Bolanos, S. (2002). Digital classification vs. visual interpretation: A case study in humid tropical forests of the Peruvian Amazon, *International Center for* Tropical Agriculture, 1, 1-5.

Roy, P. S., Dwivedi, R. S., & Vijayan, D. (Eds.) (2010). *Remote sensing applications*. National Remote Sensing Centre. Hyderabad, India.

Rwanga, S. S., & Ndambuki, J. M. (2017). Accuracy assessment of land use/land cover classification using remote sensing and GIS. *International Journal of Geosciences*, 8(4), 611–622. https://doi.org/10.4236/ijg.2017.84033

Sabree Ali, A. H., Amany, A. K., & Jalil, Mustafa. Abdul. (2020). Predicting the future growth depending on GIS and IDRISI program, City of Najaf-Iraq. *IOP Conference*

Series: Materials Science and Engineering, 881(1), 012031. https://doi.org/10.1088/1757-899X/881/1/012031

Sarkar, B., & Patra, S. (2022). A geospatial analysis of the relationship between land surface temperature and land use/land cover indices in Raiganj Municipality, West Bengal, India. *Research Square*, 1, 1-20. https://doi.org/10.21203/rs.3.rs-1497635/v1

Schulz, D., Yin, H., Tischbein, B., Verleysdonk, S., Adamou, R., & Kumar, N. (2021). Land use mapping using Sentinel-1 and Sentinel-2 time series in a heterogeneous landscape in Niger, Sahel. *ISPRS Journal of Photogrammetry and Remote Sensing*, 178, 97–111. https://doi.org/10.1016/j.isprsjprs.2021.06.005

Shahtahmassebi, A. R., Li, C., Fan, Y., Wu, Y., lin, Y., Gan, M., Wang, K., Malik, A., & Blackburn, G. A. (2021). Remote sensing of urban green spaces: A review. *Urban Forestry & Urban Greening*, 57, 1-37. https://doi.org/10.1016/j.ufug.2020.126946

Shao, X., Zhang, M., & Cai, W. (2012). Multivariate calibration of near-infrared spectra by using influential variables. *Analytical Methods*, 4(2), 467–473. https://doi.org/10.1039/C2AY05609G

Singh, R., & Preeti, K. (2017). Land transformation in the western periphery of Chandigarh: A case study using remote sensing and GIS. *International Journal of Interdisciplinary and Multidisciplinary Studies*, 4(3), 170-178.

Soares, M. G. (n.d.). Relação entre as mudanças de uso e cobertura de terra e as queimadas em florestas de miombo, Gurué, Moçambique. Master Theses, Universidade Eduardo Mondlane, Maputo, Mozambique.

Song, R., Lin, H., Wang, G., Yan, E., & Ye, Z. (2018). Improving selection of spectral variables for vegetation classification of East Dongting Lake, China, using a Gaofen-1 Image. *Remote Sensing*, 10(1), 50. https://doi.org/10.3390/rs10010050

Subedi, P., Subedi, K., & Thapa, B. (2013). Application of a hybrid cellular automaton – Markov (CA-Markov) model in land-use change prediction: A case study of Saddle Creek Drainage Basin, Florida. *Applied Ecology and Environmental Sciences*, 1(6), 126-132. https://doi.org/10.12691/aees-1-6-5

Svatonova, H. (2016). Analysis of visual interpretation of satellite data. *ISPRS - International Archives of the Photogrammetry, Remote Sensing and Spatial Information Sciences*, *XLI-B2*, 675–681. https://doi.org/10.5194/isprsarchives-XLI-B2-675-2016

Talukdar, S., Singha, P., Mahato, S., . S., Pal, S., Liou, Y.-A., & Rahman, A. (2020). Land use land cover classification by machine learning classifiers for satellite observations A Review. *Remote Sensing*, 12, 1-24. https://doi.org/10.3390/rs12071135

Tariq, A., Yan, J., & Mumtaz, F. (2022). Land change modeler and CA-Markov chain analysis for land use land cover change using satellite data of Peshawar, Pakistan. *Physics and Chemistry of The Earth*, 128, 15. https://doi.org/10.1016/j.pce.2022.103286

Tempfli, K., Huurneman, G. C., Bakker, W. H., Janssen, L. L. F., Feringa, W. F., Gieske, A. S. M., Grabmaier, K. A., Hecker, C. A., Horn, J. A., Kerle, N., Meer, F. D. van der, Parodi, G. N., Pohl, C., Reeves, C. V., Ruitenbeek, F. J. A. van, Schetselaar, E. M., Weir, M. J. C., Westinga, E., & Woldai, T. (2009). *Principles of remote sensing: An introductory textbook*. ITC Educational Textbook Series, vol. 2, International Institute for Geo-Information Science and Earth Observation, Enschede. http://www.itc.nl/library/papers_2009/general/PrinciplesRemoteSensing.pdf

Thiam, S., Villamor, G. B., Faye, L. C., Sène, J. H. B., Diwediga, B., & Kyei-Baffour, N. (2021). Monitoring land use and soil salinity changes in coastal landscape: A case study from Senegal. *Environmental Monitoring and Assessment*, 193(5), 259. https://doi.org/10.1007/s10661-021-08958-7

Tibebe, M., Kumar, L., Koech, R., & Kogo, B. (2020). Mapping of land-use land-cover changes and its dynamics in Awash River Basin using remote sensing and GIS. *Remote Sensing Applications: Society and Environment*, 19, 100352. https://doi.org/10.1016/j.rsase.2020.100352

Todorovski, D., Zevenbergen, J., van der Molen, P., & Groenendijk, L. (2013). Post-conflict land administration and its current status as facilitator of the post-conflict state building; case Mozambique. *Environment for Sustainability*, 1-11.

Tomaszewski, M., Gasz, R., & Smykała, K. (2021). Monitoring vegetation changes using satellite imaging – NDVI and RVI4S1 indicators. In: Paszkiel, S. (eds) Control, Computer Engineering and Neuroscience. *Springer - Advances in Intelligent Systems and Computing*, 1362, 268–278. https://doi.org/10.1007/978-3-030-72254-8_29

Tsoeleng, L. T., Odindi, J., Mhangara, P., & Malahlela, O. (2020). Assessing the performance of the multi-morphological profiles in urban land cover mapping using pixel based classifiers and very high resolution satellite imagery. *Scientific African*, 10, e00629. https://doi.org/10.1016/j.sciaf.2020.e00629

Tuzine, M. S. (2011). Mapeamento da cobertura e uso da terra a partir de imagens Ikonos na Floresta de Inhamacari, Província de Manica—Moçambique. Master Theses, Universidade Federal do Paraná, Curitiba, Brasil. https://acervodigital.ufpr.br/handle/1884/26458

Twisa, S., & Buchroithner, M. F. (2019). Land-use and land-cover change detection in Wami River Basin, Tanzania. *Land*, 8(9), 136. https://doi.org/10.3390/land8090136

Wang, L., Wang, J., Liu, Z., Zhu, J., & Qin, F. (2022). Evaluation of a deep-learning model for multispectral remote sensing of land use and crop classification. *The Crop Journal*,10(5), 1435-1451. https://doi.org/10.1016/j.cj.2022.01.009

Woodcock, C. E., Loveland, T. R., Herold, M., & Bauer, M. E. (2020). Transitioning from change detection to monitoring with remote sensing: A paradigm shift. *Remote Sensing of Environment*, 238, 111558. https://doi.org/10.1016/j.rse.2019.111558

Yadav, Y., Chhetri, B., Rayamajhi, S., Tiwari, K., & Sitaula, B. (2019). Dynamics of land use land cover change and mapping of tree outside forest (TOF) in Terai, Nepal. *International Journal of Environmental Sciences & Natural Resources*, 19(1), 556002. https://doi.org/10.19080/IJESNR.2019.19.556002

Yesuph, A. Y., & Dagnew, A. B. (2019). Land use/cover spatiotemporal dynamics, driving forces and implications at the Beshillo catchment of the Blue Nile Basin, North Eastern Highlands of Ethiopia. *Environmental Systems Research*, 8(1), 21. https://doi.org/10.1186/s40068-019-0148-y

Zandi, B., & Chaure, S. (2015). Assessment of land degradation due to opencast mining using remote sensing and GIS. *Indian Research Communication*, l9(1), 68–73.

Zvobgo, L., & Tsoka, J. (2021). Deforestation rate and causes in upper Manyame Sub-Catchment, Zimbabwe: Implications on achieving national climate change mitigation targets. *Trees, Forests and People*, 5, 100090. https://doi.org/10.1016/j.tfp.2021.100090

APPENDIX A.

Table A. 1. Statistical data of the population evolution between 1980 and 2020, their percentage change, rate of change, density and projection for 2050

Year	Population	Net Increase	% Increase	Annual Increase	Average Growth Rate	Years	Density
1980	39296						48
1990	40320	1 024	0.03	102	0.26%	10	49
2000	61446	21 126	0.52	2113	4.21%	10	75
2010	121538	60 093	0.98	6009	6.82%	10	148
2020	244369	122 831	1.01	12283	6.98%	10	298
2030	346027	101 658	0.42	10166	3.48%	10	422
2040	456910	110 883	0.32	11088	2.78%	10	557
2050	572793	115 883	0.25	11588	2.26%	10	699
1980-2020		205 073	5.22	5127	4.57%	40	
1980-2050		533 497	13.58	7621	3.83%	70	
2020-2050		328 424	1.34	10947	2.84%	30	

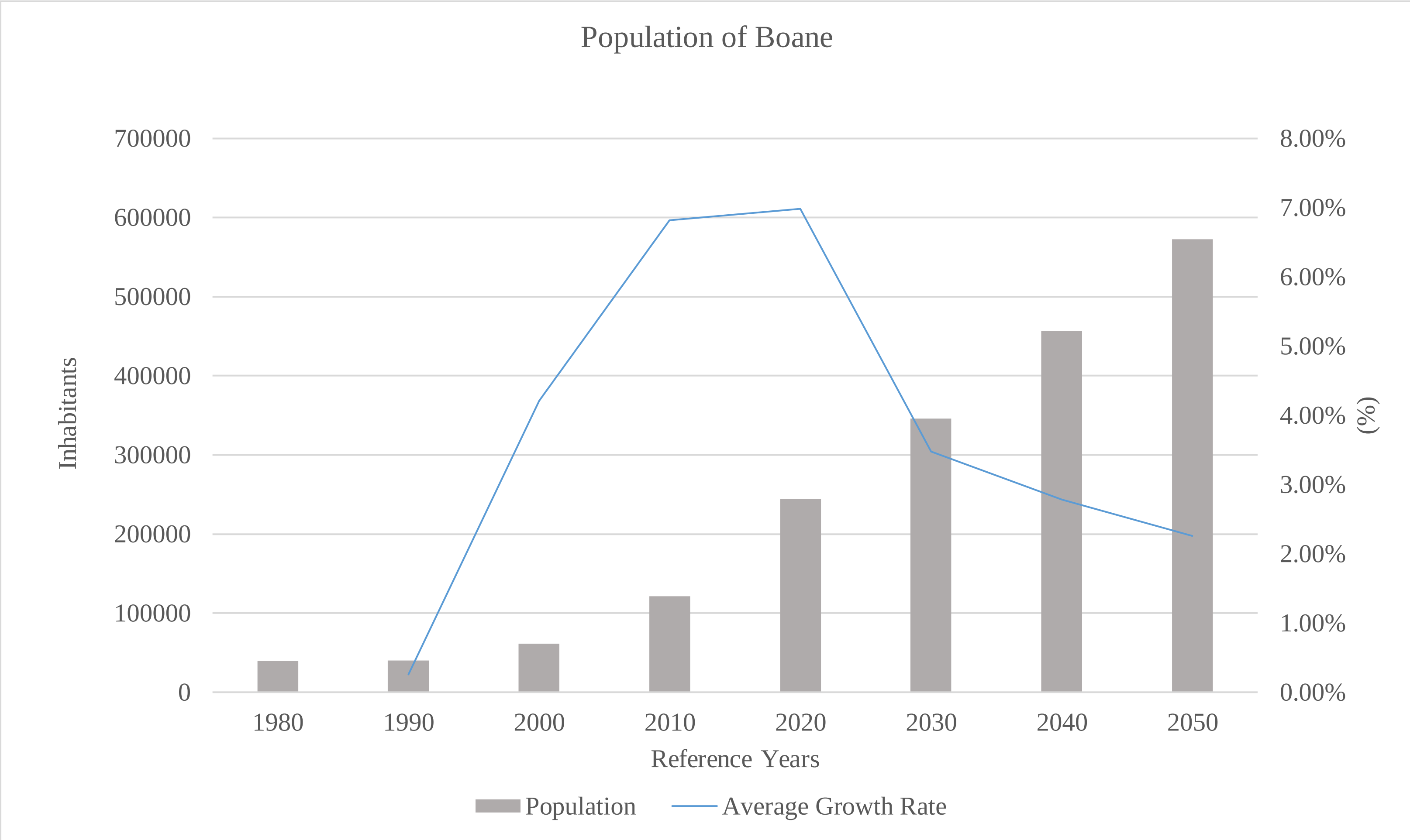

Figure A 1. Population growth between 1980 and 2020 and projections for 2050

APPENDIX B.

Table B. 1. Detailed outputs of short-term change detection analyse comparing ten years, showing values of persistence, gains and loss, between 1984 and 1990

1984	1990							Total	Loss
Sq.km	Agriculture	Barren	Build-up	Forest	Rock	Waterbody	Wetland		
Agriculture	69.9	11.3	3.3	78.4	18.4	2.7	34.1	218.1	148.2
Barren	46.3	4.9	4.9	24.0	11.3	2.9	5.3	99.5	94.6
Build-up	0.7	0.2	0.8	0.0	0.2	0.2	0.2	2.3	1.6
Forest	39.5	11.1	6.7	212.8	11.6	0.9	37.0	319.5	106.7
Rock	10.5	0.2	0.5	21.5	41.2	0.6	0.0	74.5	33.3
Water Body	1.4	0.0	0.0	0.1		6.7	0.8	8.9	2.2
Wet Land	6.6	4.3	0.4	18.7	1.3	1.0	48.7	81.0	32.3
Total	174.9	32.0	16.6	355.4	84.0	14.9	126.0	803.8	418.9
Gain	105.0	27.1	15.8	142.6	42.9	8.2	77.3		

Table B. 2. Detailed outputs of short-term change detection analyse comparing ten years, showing values of persistence, gains and loss, between 1990 and 2000

1990	2000							Total	Loss
Sq.km	Agriculture	Barren	Build-up	Forest	Rock	Waterbody	Wetland		
Agriculture	62.6	16.4	20.5	57.4	14.0	1.4	2.6	174.9	112.3
Barren	5.5	0.8	10.6	8.8	0.2	0.1	6.0	32.0	31.2
Build-up	3.5	5.1	5.3	1.7	0.5	0.0	0.5	16.6	11.2
Forest	75.7	37.8	31.4	168.9	19.9	0.4	21.4	355.4	186.5
Rock	17.7	13.6	1.0	18.4	33.4	0.0	0.0	84.0	50.6
Waterbody	0.0	0.0	0.0	0.0	0.0	14.0	0.9	14.9	0.9
Wetland	11.9	0.6	25.2	35.7	0.0	1.4	51.1	126.0	74.9
Total	177.0	74.3	94.0	291.0	68.0	17.2	82.4	803.8	467.7
Gain	114.4	73.5	88.7	122.1	34.6	3.2	31.3		

Table B. 3. Detailed outputs of short-term change detection analyse comparing ten years, showing values of persistence, gains and loss, between 2000 and 2010

2000	2010							Total	Loss
Sq.km	Agriculture	Barren	Build-up	Forest	Rock	Waterbody	Wetland		
Agriculture	25.9	55.9	36.8	45.4	11.5	0.5	1.0	177.0	151.1
Barren	5.9	29.3	13.4	20.8	4.3	0.0	0.6	74.3	45.0
Build-up	3.6	31.3	40.1	12.9	0.5	0.1	5.5	94.0	53.9
Forest	22.4	56.5	27.8	146.1	20.7	0.2	17.3	291.0	145.0
Rock	5.7	7.3	1.2	9.2	44.5	0.0	0.0	68.0	23.5
Waterbody	0.4	0.1	0.1	0.2	0.0	15.1	1.4	17.2	2.1
Wetland	2.6	4.3	3.9	13.7	0.0	4.7	53.2	82.4	29.2
Total	66.5	184.7	123.2	248.2	81.4	20.7	79.0	803.9	449.8
Gain	40.6	155.4	83.1	102.2	36.9	5.6	25.9		

Table B. 4. Detailed outputs of short-term change detection analyse comparing ten years, showing values of persistence, gains and loss, between 2010 and 2020

2010	2020							Total	Loss
Sq.km	Agriculture	Barren	Build-up	Forest	Rock	Waterbody	Wet Land		
Agriculture	5.4	12.5	15.5	14.6	15.4	0.0	3.2	66.5	61.2
Barren	0.2	45.3	115.5	10.9	2.9	0.0	9.9	184.7	139.4
Build-up	0.2	7.0	104.0	7.2	0.0	0.1	4.7	123.2	19.2
Forest	0.3	38.7	109.9	79.9	9.1	0.2	10.2	248.2	168.3
Rock	0.2	4.7	2.8	2.5	70.3	0.0	1.0	81.4	11.2
Waterbody	1.3	0.0	0.0	4.0	3.9	11.3	0.1	20.7	9.4
Wetland	0.8	6.6	22.9	28.0	0.1	1.4	19.3	79.0	59.8
Total	8.3	114.8	370.7	147.0	101.7	13.1	48.3	803.8	468.4
Gain	2.9	69.5	266.7	67.0	31.4	1.7	29.0		

Table B. 5. Detailed outputs of long-term change detection analyse comparing 36 years, showing values of persistence, gains and loss, swapping areas, changes and shares, between 1984 and 2020

1984	2020							Total	Loss
Sq.km	Agriculture	Barren	Build-up	Forest	Rock	Water Body	Wet Land		
Agriculture	2.0	33.4	127.5	24.8	17.8	1.1	11.4	218.1	216.1
Barren	1.0	15.7	47.9	9.5	20.6	1.3	3.4	99.5	83.8
Build-up	0.1	0.3	0.6	0.5	0.6	0.2	0.1	2.3	1.8
Forest	2.2	49.0	170.3	72.7	11.1	0.7	13.6	319.5	246.8
Rock	0.2	9.7	12.5	2.4	48.1	0.1	1.5	74.5	26.4
Water Body	0.2	0.0	0.0	0.8	0.0	7.8	0.0	8.9	1.2
Wet Land	2.6	6.8	11.9	36.3	3.4	1.7	18.2	81.0	62.8
Total	8.3	114.8	370.7	147.0	101.7	13.1	48.3	803.8	638.8
Gain	6.3	99.1	370.1	74.3	53.5	5.3	30.1	638.8	

Table B. 6. Detailed outputs of long-term change detection analyse comparing 30 years, showing values of persistence, gains and loss, swapping areas, changes and shares, between 2020 and 2050

Sq.km	2050							Total	Loss
2020	Agriculture	Barren	Build-up	Forest	Rock	Water Body	Wet Land		
Agriculture	2.12	0.30	4.59	0.41	0.66	0.02	0.18	8.3	6.2
Barren	0.01	54.38	50.96	5.84	0.00	0.05	3.55	114.8	60.4
Build-up	0.02	10.19	345.84	4.37		0.07	10.18	370.7	24.8
Forest	0.19	9.50	52.15	78.64	1.00	0.45	4.95	146.9	68.2
Rock	0.02	8.06	17.75	1.05	73.32	0.03	1.44	101.7	28.3
Water Body	0.82	0.25	1.51	2.56	3.30	4.48	0.08	13.0	8.5
Wet Land	0.02	2.59	14.14	4.83		0.09	26.60	48.3	21.7
Class Total	3.2	85.3	486.9	97.7	78.3	5.2	47.0	803.6	218.2
Gain	1.1	30.9	141.1	19.1	5.0	0.7	20.4	218.2	218.2

APPENDIX C.

https://code.earthengine.google.com/?accept_repo=users/CDengo/Image2010

Figure C. 1. Google Earth engine code